ADVANCED FUNCTIONAL MATERIALS
www.afm-journal.de

Stretchable, Skin-Mountable, and Wearable Strain Sensors and Their Potential Applications: A Review

Morteza Amjadi, Ki-Uk Kyung, Inkyu Park, and Metin Sitti**

There is a growing demand for flexible and soft electronic devices. In particular, stretchable, skin-mountable, and wearable strain sensors are needed for several potential applications including personalized health-monitoring, human motion detection, human-machine interfaces, soft robotics, and so forth. This Feature Article presents recent advancements in the development of flexible and stretchable strain sensors. The article shows that highly stretchable strain sensors are successfully being developed by new mechanisms such as disconnection between overlapped nanomaterials, crack propagation in thin films, and tunneling effect, different from traditional strain sensing mechanisms. Strain sensing performances of recently reported strain sensors are comprehensively studied and discussed, showing that appropriate choice of composite structures as well as suitable interaction between functional nanomaterials and polymers are essential for the high performance strain sensing. Next, simulation results of piezoresistivity of stretchable strain sensors by computational models are reported. Finally, potential applications of flexible strain sensors are described. This survey reveals that flexible, skin-mountable, and wearable strain sensors have potential in diverse applications while several grand challenges have to be still overcome.

1. Introduction

Skin-mountable and wearable electronic devices have recently attracted tremendous attention due to their facile interaction with human body and long-term monitoring capabilities. Physical, chemical, biological, and environmental status of the human body could be monitored by various flexible sensors with high efficiency and minimum discomfort.[1–9] Skin-mountable and wearable sensors can be attached onto the clothing or even directly mounted on the human skin for the real-time monitoring of human activities.[10] Besides their high efficiency, they must fulfill several minimum requirements including high stretchability, flexibility, durability, low power consumption, biocompatibility, and lightweight. These demands become even more severe for epidermal electronic devices where mechanical compliance like human skin and high stretchability ($\varepsilon > 100\%$ where ε is the strain) are required.[11,12] Recently, several types of skin-mountable and wearable sensors have been proposed by using nanomaterials coupled with flexible and stretchable polymers. Indeed, nanomaterials are utilized as functional sensing elements owing to their outstanding electrical, mechanical, optical, and chemical properties while polymers are employed as flexible support materials thanks to their flexibility, stretchability, human-friendliness, and durability.[13] Examples of those innovative sensors include strain sensors,[10,12–14] pressure sensors,[5,15–17] electronic skins (e-skins),[3,16–20] and temperature sensors.[2,21,22] Particularly, various skin-mountable and wearable strain sensors have been developed because of their broad applications in personalized heath-monitoring, human motion detection, human-machine interfaces, and soft robotics.[10,12,23–31]

This paper aims to survey fabrication processes, working mechanisms, strain sensing performances, and applications of stretchable strain sensors. The article is organized as follows: first, common operation mechanisms of stretchable strain sensors are described. Here, we summarize novel functional nanomaterials and techniques for the fabrication of stretchable strain sensors in details. Second, mechanisms involved in the strain-responsive behavior of resistive-type and capacitive-type sensors are explained. We show that the influence of traditional mechanisms like geometrical changes and piezoresistivity of materials on the strain sensing performance of flexible strain sensors are very small whereas mechanisms such as disconnection between sensing elements, crack propagation in thin films, and tunneling effect can potentially be employed for highly stretchable and sensitive strain sensing. Third, we emphasize the performance parameters of stretchable strain sensors in terms of stretchability, sensitivity, linearity, hysteresis behavior, response time, overshooting, and durability. We demonstrate

M. Amjadi, Prof. M. Sitti
Physical Intelligence Department
Max-Planck Institute for Intelligent Systems
Heisenbergstr. 3
Stuttgart 70569, Germany
E-mail: sitti@is.mpg.de

Dr. K.-U. Kyung
Transparent Transducer and UX Creative Research Center
Electronics and Telecommunication Research Institute (ETRI)
218 Gajeong-ro, Yuseong-gu
Daejeon 34129, South Korea

Prof. I. Park
Department of Mechanical Engineering
Korea Advanced Institute of Science & Technology (KAIST)
291 Daehak-ro, Yuseong-gu, Daejeon 34141, South Korea
E-mail: inkyu@kaist.ac.kr

DOI: 10.1002/adfm.201504755

that the selection of appropriate polymers and their interaction with functional nanomaterials are essential for excellent and reliable dynamic strain sensing. Fourth, recent computational models for the simulation of the piezoresistivity of stretchable strain sensors are reported. Fifth, we highlight the potential applications of stretchable and sensitive strain sensors. Next section describes current challenges in the use of flexible, skin-mountable, and wearable sensors, especially, for body-integrated applications. Last section provides conclusions and future remarks of stretchable strain sensors.

2. Flexible Strain Sensors

Strain sensors transduce mechanical deformations into electrical signals. Flexible and stretchable strain sensors could mainly be classified into resistive-type and capacitive-type sensors. Although there are several other types of strain sensors including fiber Bragg grating (FBG), Raman shift, liquid metals, triboelectricity, and piezoelectricity based strain sensors,[32–41] practical implementation of these strain sensors for skin-mountable and wearable applications remains still challenging largely due to their sophisticated measurement equipment, low resolution, and poor dynamic performance.[32–38,42–45] On the other hand, resistive-type and capacitive-type sensors require relatively simple read-out systems and offer high flexibility and stretchability.[10,14,33,46,47] In this article, therefore, we keep our focus on resistive-type and capacitive-type sensors only. Resistive-type sensors are typically composed of electrically conductive sensing films coupled with flexible substrates. When composite structures are stretched, microstructural changes in the sensing films lead to the change of electrical resistance as a function of the applied strain. After release of the strain, reestablishment of the sensing films to their original states recovers the electrical resistance of sensors. Capacitive-type sensors employ a highly compliant dielectric layer sandwiched between a pair of stretchable electrodes. Tensile strain brings two electrodes closer and results in an increase of capacitance. **Figure 1** illustrates several flexible, skin-mountable, and wearable strain sensors made of functional nanomaterials and stretchable polymer composites.

One important consideration is the choice of suitable materials and methods for the fabrication of flexible strain sensors. Fabrication process of flexible sensors should be low-cost and scalable, enabling large-area and facile production. To date, stretchable strain sensors have been fabricated by using low-dimensional carbons (e.g., carbon blacks (CBs), carbon nanotubes (CNTs), and graphene),[12,14,33,47–63] nanowires (NWs),[10,29,64–66] nanoparticles (NPs),[67–70] and their hybrid micro/nanostructures.[62,71–75] Silicone-based elastomers (e.g., polydimethylsiloxane (PDMS), Ecoflex, and Dragon Skin)[10,12,14,29,33,47,52,53,55–57,60,65,67,71,76] and rubbers (e.g., natural rubber and thermoplastic elastomers (TPEs))[48,49,51,54,59,61,62,72,74,77,78] are the most commonly used polymers as flexible support materials of soft strain sensors. Although the influence of polymer types on the piezoresistivity of low-strain gauges was noticed to be relatively small,[42] the importance of appropriate polymer support for the high performance strain sensing will be discussed later.

Morteza Amjadi received his B.Sc. degree in Engineering at Iran University of Science and Technology (IUST), Tehran, Iran, in 2012, and his M.Sc. degree in Mechanical Engineering at Korea Advanced Institute of Science and Technology (KAIST), Daejeon, South Korea, in 2014. After graduation from KAIST, he joined the Electronics and Telecommunication Research Institute (ETRI), Daejeon, South Korea, as a researcher. He is currently a Ph.D. student in the Physical Intelligence Department and Max Planck-ETH Center for Learning Systems under the supervision of Prof. Metin Sitti. His research interests include soft and smart materials, towards the development of flexible electronic devices (e.g., sensors, actuators, soft robots, etc.)

Inkyu Park received his B.S., M.S. and Ph.D. degrees at KAIST (1998), UIUC (2003) and at UC Berkeley (2007), respectively, all in Mechanical Engineering. He has worked as a research specialist at Berkeley Sensor and Actuator Center (2007–2008) and a visiting researcher at Hewlett Packard Laboratory (2005–2008). He is currently an associate professor at the department of mechanical engineering at KAIST. His main research interests are printed electronics, hybrid micro/nanofabrication, nanomaterial-based chemical and physical sensors, and mechanical reliability of micro/nano devices.

Metin Sitti received his B.Sc. and M.Sc. degrees in Electrical and Electronics Engineering from Bogazici University, Turkey, in 1992 and 1994, respectively, and his Ph.D. degree in Electrical Engineering from the University of Tokyo, Japan, in 1999. He was a research scientist at the University of California at Berkeley during 1999–2002. He is currently a director of the Physical Intelligence Department at the Max-Planck Institute for Intelligent Systems, Stuttgart, Germany and a professor at Carnegie Mellon University, Pittsburgh, USA. His research interests include small-scale physical intelligence, mobile milli- and microrobots, soft materials and robots, bio-inspired materials, and medical miniature robots.

DOI: 10.1002/adfm.201504755

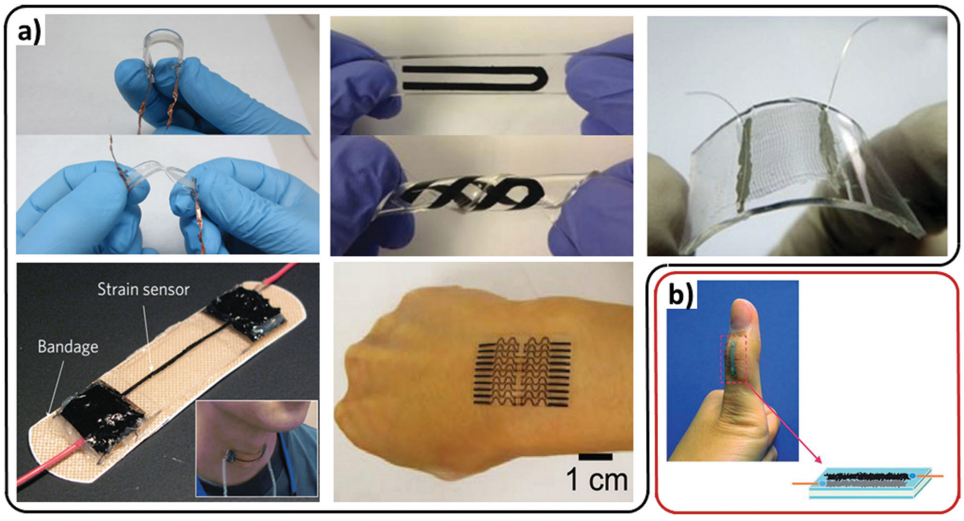

Figure 1. Various flexible, skin-mountable, and wearable strain sensors made of functional nanomaterials-polymer composites. a) Resistive-type sensors, and b) capacitive-type sensors. a) Reproduced with permission.[10] Copyright 2014, American Chemical Society. Reproduced with permission.[12] Reproduced with permission.[14] Copyright 2011, Nature Publishing Group. Reproduced with permission.[47] Reproduced with permission.[76] Copyright 2012, Nature Publishing Group. b) Reproduced with permission.[65] Copyright 2013, Royal Society of Chemistry.

Stretchable strain sensors were fabricated through different processes including filtration method,[10,47,58,71,73,79,80] printing technology,[57,65,66,71] transferring and micromolding methods,[14,50,52,55,56,58,60] coating techniques,[49,54,61,63,72,78,79] liquid phase mixing,[12,51,52,60,62,71,77,81] and chemical synthesis methods.[14,55,56,76,82] We have recently reported highly stretchable and sensitive strain sensors based on the silver nanowires (AgNWs)-elastomer nanocomposites.[10,64] The AgNW network thin films were first coated on a donor substrate and then were transferred to the PDMS matrix by filtration technique (**Figure 2**a).[10,83,84] The robust nanocomposites of AgNW fillers and PDMS matrix with different network densities were then tested for strain sensing. Hempel et al. demonstrated flexible and sensitive strain sensors by spray coating of graphene flakes on polyethylene terephthalate (PET) substrates (Figure 2b).[54] Properties of thin films such as transparency and electrical conductivity were controlled by the amount of the sprayed solution. In another approach, chemical vapor deposition (CVD) method was utilized for direct growth of CNT and graphene thin films. In this method, carbon feedstock gases were supplied on a substrate decorated with catalyst particles under high temperature condition (> 800 °C). The grown thin films were then transferred to flexible substrates by different transfer techniques.[55,85] For instance, graphene thin films grown on the Ni catalyst layer were transferred to the PDMS substrate by PDMS stamps. The resulting graphene-PDMS composites were characterized for strain sensing (Figure 2c).[55] Highly stretchable and soft strain sensors were reported by Muth et al. using embedded 3D printing technique where the viscous nanomaterial ink was directly embedded in elastomer films through a deposition nozzle (Figure 2d).[57] Figure 2e illustrates the solution mixing procedure for the fabrication of nanocomposite structures. Nanomaterial fillers and liquid-phase polymers are vigorously mixed together to obtain nanocomposite structures. Kong et al. reported stretchable sensors based on the CBs-PDMS nanocomposite films prepared by the solution mixing method.[52] Cohen et al. reported a highly elastic capacitive-type sensor based on the percolation network of CNTs. The CNT percolation network thin films were transfer-printed onto silicone dielectric layers.[58] In another approach, the patterned AgNW percolation networks were transferred to PDMS by filtration method.[65,79] The AgNWs–PDMS nanocomposites formed highly stretchable and stable electrodes. Then, two opposite stretchable electrodes were brought together with a laminated Ecoflex dielectric layer.[65] Highly transparent and stretchable strain sensors were demonstrated by Cai et al. using transparent CNT percolation thin films synthesized by the floating catalyst chemical vapor deposition (FCCVD) method.[33] The conductance and optical transparency of thin films were controlled by the growth parameters. Stretchable electrodes were typically made of the percolation network of one-dimensional (1D) nanomaterials (e.g., CNTs and AgNWs) that maintain stable and reliable electromechanical properties at high strains.[33,53,58,65,79,86] For detailed fabrication processes of flexible electronic devices, we refer the reader to the following review papers.[6,8,85,87–89]

3. Strain-Responsive Mechanism

Strain sensors respond to the applied strain with different mechanisms, depending on the type of materials, micro/nanostructures, and fabrication process. Strain-resistance response of traditional strain gauges originates from geometrical effects and piezoresistivity of materials themselves. Unlike traditional strain gauges, mechanisms such as disconnection between sensing elements, crack propagation in thin films, and tunneling effect have been utilized to develop stretchable strain sensors.

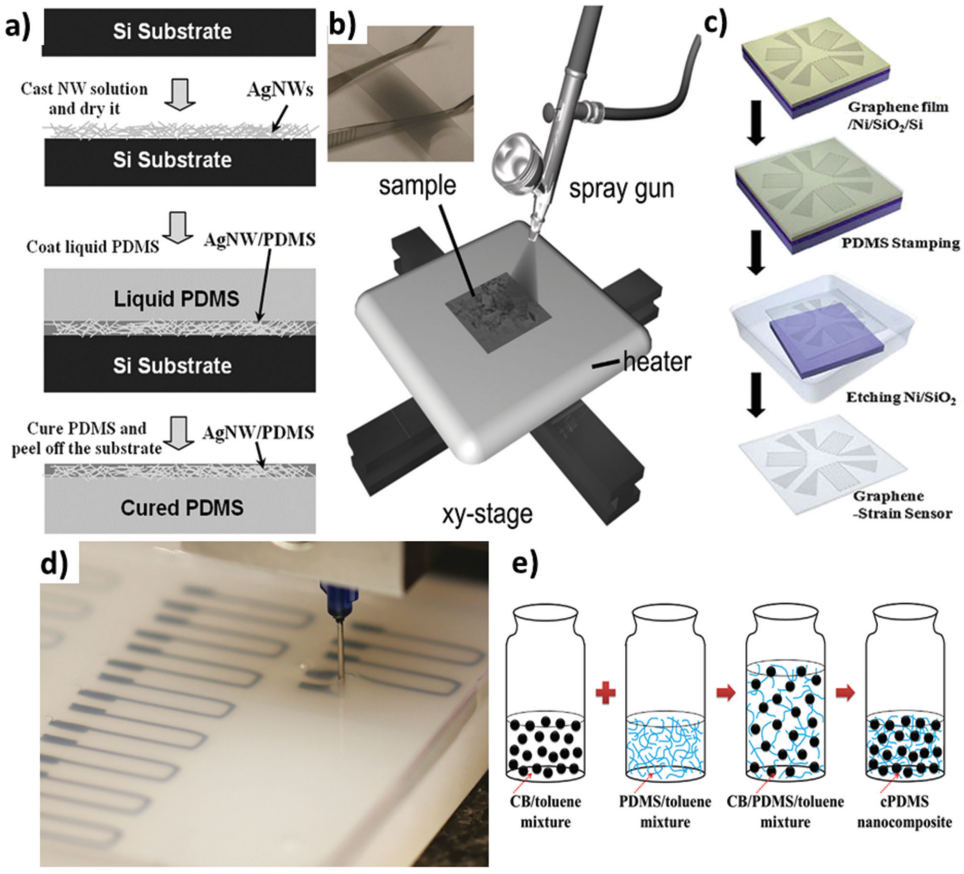

Figure 2. Fabrication processes of stretchable strain sensors. a) Filtration method; transferring thin films from a donor substrate to a polymer-targeted substrate by penetration of the liquid polymers. Reproduced with permission.[83] b) Coating technique; coating of material solutions on the top of flexible polymers to form nanomaterial thin films-polymer composites; inset: graphene thin film air-spray coated on the PET substrate. Reproduced with permission.[54] Copyright 2012, American Chemical Society. c) Transferring process; transmitting thin films from one substrate to another substrate by using an intermediate substrate. Reproduced with permission.[55] Copyright 2013, Elsevier. d) Printing technology; printing nanomaterial inks onto flexible polymer substrates by deposition nuzzles. Reproduced with permission.[57]. e) Solution mixing; fabrication of nanomaterial fillers-polymers nanocomposites. Reproduced with permission.[52] Copyright 2014, Elsevier.

3.1. Geometrical Effect

When materials are stretched, they tend to contract in transverse direction of stretching based on the Poisson's ratio of υ. For a conductor, the resistance is given by $R = \rho L/A$, where ρ is the electrical resistivity, L is the length, and A is the cross-sectional area of the conductor. Resistance of a conductor increases upon elongation in length and shrinkage in cross-sectional area. Dimensional changes are the piezoresistive and piezocapacitance mechanisms of commercially available metal-based resistive-type and stretchable capacitive-type sensors, respectively.[54,90] Upon stretching, capacitive-type sensors sustain change of capacitive area and decrease in the thickness of the dielectric layer, resulting in an increase of capacitance.[33,58,65,86] Consider a parallel-plate capacitor with initial length (l_0), width (w_0), and thickness (d_0) of the dielectric layer. The initial capacitance C_0 is given by:

$$C_0 = \varepsilon_0 \varepsilon_r \frac{l_0 w_0}{d_0} \tag{1}$$

where ε_0 and ε_r donate dielectric constant of vacuum and relative permittivity of dielectric media, respectively. When the sensor is stretched to a given strain ε, the length of capacitor increases to $(1+\varepsilon)l_0$ while the width and thickness of dielectric layer decrease to $(1-\nu_{\text{electrode}})w_0$ and $(1-\nu_{\text{dielectric}})d_0$ where $\nu_{\text{electrode}}$ and $\nu_{\text{dielectric}}$ are the Poisson's ratios for the stretchable electrodes and dielectric layer, respectively. For stretchable strain sensors, if we assume that both stretchable electrodes and dielectric layer have same Poisson's ratio, then the capacitance upon stretching could be calculated as:

$$C = \varepsilon_0 \varepsilon_r \frac{(1+\varepsilon) l_0 (1-\nu_{\text{electrode}}) w_0}{(1-\nu_{\text{dielectric}}) d_0} = \varepsilon_0 \varepsilon_r \frac{(1+\varepsilon) l_0 w_0}{d_0} = (1+\varepsilon) C_0 \tag{2}$$

Here, the capacitance of capacitive-type sensors increases as a linear function of the applied strain. It should be noted that this linear function is limited to a certain amount of strain. If the applied strain is too large, linear relationship between different axes via the Poisson's ratio is not valid anymore for the utilized polymer.

Adv. Funct. Mater. 2016,
DOI: 10.1002/adfm.201504755

3.2. Piezoresistive Effect

Change in the resistance of materials caused by the structural deformations is known as piezoresistivity. In this case, the relative change of resistance could be written as: $\Delta R/R = (1 + 2\upsilon)\varepsilon + \Delta\rho/\rho$. The former term expresses the influence of geometrical changes, while latter indicates the piezoresistivity of materials themselves. Piezoresistivity of some metals and metal-alloys may increase the resistance of strain gauges to few times whereas semiconductor materials such as silicon and germanium can enhance the resistance change of sensors to several orders of magnitudes, induced by the change of the bandgap on inter-atomic spacing.[12,90–94] In addition, nanoscale materials such as individual CNT and zinc oxide nanowire (ZnONW) showed ultrahigh piezoresistivity owning to their chirality and change in barrier height, respectively.[34,49,82,90,92,95–99] Therefore, highly sensitive strain gauges could be achieved by semiconductors or nanoscale materials. However, the stretchability of skin-mountable and wearable strain sensors ($\varepsilon > 50\%$) far exceeds the measurement limit of conventional strain gauges made of metals and semiconductors ($\varepsilon \leq 5\%$).[47,54] Moreover, technical difficulties, inhomogeneous electromechanical properties, and poor stretchability have prevented the widespread use of single nanotube or nanowire as strain sensors. To overcome these shortcomings, unlike traditional strain sensing mechanisms, several new approaches have been proposed for achieving highly stretchable and sensitive strain sensors by forming composites of functional nanomaterials and stretchable polymers. Even in this case, the contribution of the piezoresistivity of nanomaterials on the total resistance-strain behavior of stretchable strain sensors may be expected to be low due to the large elastic mismatch as well as weak interfacial adhesion strength between nanomaterials and polymers, yielding negligible deformations of nanomaterials upon stretching.[10,32,34,42,90,100]

3.3. Disconnection Mechanism

In conductive thin films made of nanomaterial conductive network, electrons can pass through overlapped nanomaterials within the percolation network. Stretching of thin films causes some connected nanomaterials to lose their overlapped area and electrical connection, consequently, increases the electrical resistance. In microstructural point of view, disconnection of overlapped nanomaterials under stretching is caused by the slippage of nanomaterials due to the weak interfacial binding and large stiffness mismatch between nanomaterials and stretchable polymers.[10,42,100] Stretchable and sensitive strain sensors were reported using thin films of NW networks and graphene flakes based on the disconnection mechanism.[10,29,54,61,63,75,90] We investigated the strain sensing mechanism of AgNWs–PDMS nanocomposites.[10,64] AgNWs with tensile strength of 0.92%–1.64% and Young's modulus of 81–176 GPa were embedded on a much softer PDMS layer with Young's modulus of 0.4–3.5 MPa.[10,83,101,102] Under stretching cycle, AgNW fillers slid inside the PDMS matrix due to much larger elongation of the PDMS matrix. Sliding of NWs resulted in disconnection at some NW-NW junctions. More stretching led to more disconnection between NWs and thus increased the electrical resistance. Similar mechanism was identified for the piezoresistivity of ZnONW thin films coated on PDMS substrates.[29] Another class of strain sensors was reported by graphene flakes coated on flexible support materials. When composite films were stretched, graphene flakes slid in the direction of elongation, decreased the overlapped area between connected flakes and increased the contact resistance in the flake-flake junctions.[47,54,63] Recently, few microstructure based (e.g., interlocked microstructure) strain sensors were also reported.[5,103] Here, rather than disconnection between overlapped nanomaterials upon stretching, microstructural deformation was utilized to change the output electrical signal. For instance, when two opposing conductive interlocked microdome arrays were laminated and stretched in the lateral direction, the contact area between the microdomes was dramatically decreased, which led to considerable increase in the electrical resistance.[103]

3.4. Crack Propagation

Cracks originate and propagate in brittle thin films coated on the top of soft polymer layers upon stretching. Indeed, cracks intend to initiate at the stress concentrated areas to release the accommodated stress. Microcracks were generated in CNT, silver nanoparticle (AgNP), gold nanowire (AuNW), and graphene thin films coated on flexible substrates under stretching.[10,14,56,63,67,104,105] Stretching led opening and enlargement of microcracks in thin films, critically limiting the electrical conduction through thin films due to the separation of several microcrack edges.[106] Moreover, the electrical resistance of thin films drastically increased by the applied strain. This mechanism was employed to develop highly sensitive and flexible strain sensors. **Figures 3**a and 3b show microcrack opening in the AgNP and CNT thin films under stretching, respectively.[14,76] Figure 3c depicts the in situ tracking of microstructure morphology of the graphene thin film–PDMS composite film under various strains. The density and size of microcracks were increased by the applied strain and recovered to their initial states after release of thin films. Moreover, microcrack edges were reconnected upon release of the applied strain, ensuring complete recovery of the electrical resistance.[76]

3.5. Tunneling Effect

Crossing of electrons through a nonconductive barrier is called tunneling. Electrons can tunnel through closely spaced adjacent nanomaterials.[10,34,71,107] Very thin insulating polymer layers were experimentally observed in the CNTs-polymer nanocomposites where several CNT-CNT junctions were separated from direct electrical connection, but with possible tunneling conduction.[35,42,108] Within a certain cut-off distance between neighboring nanomaterials, electrons can path through polymer thin layers and form quantum tunneling junctions. The tunneling resistance between two adjacent nanomaterials can be approximately estimated by Simmons's theory for tunneling resistance:[10,34,42]

$$R_{\text{tunnel}} = \frac{V}{AJ} = \frac{h^2 d}{Ae^2\sqrt{2m\lambda}} \exp\left(\frac{4\pi d}{h}\sqrt{2m\lambda}\right) \quad (3)$$

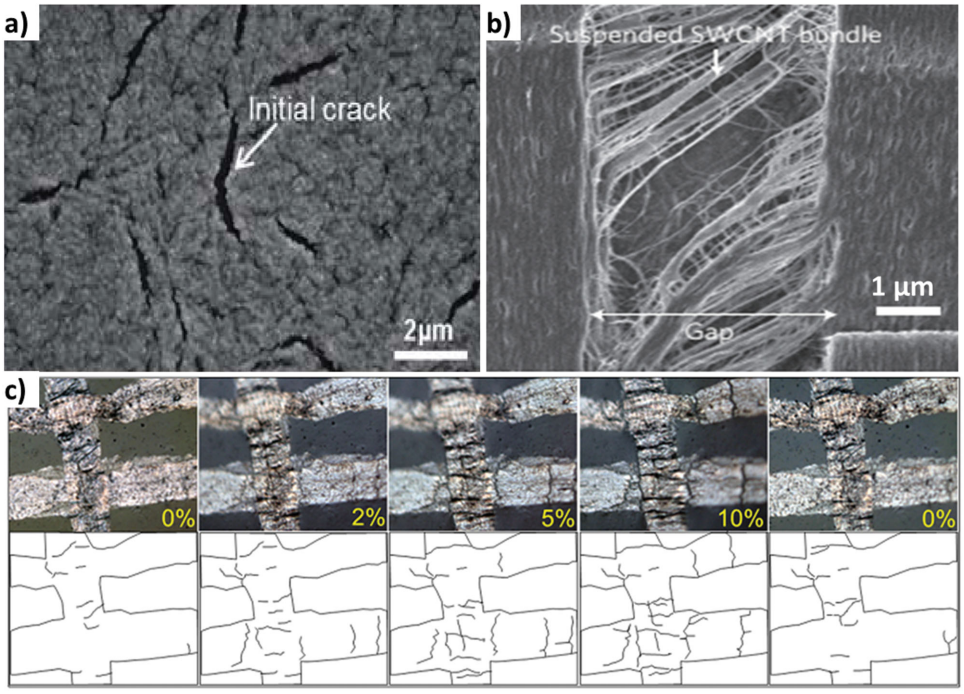

Figure 3. Microcrack generation in thin films coated on flexible support materials. a) Microcrack opening in the AgNP thin film patterned on the PDMS substrate upon stretching. Reproduced with permission.[67] Copyright 2014, Royal Society of Chemistry. b) Gap opening in the aligned CNT thin film by the elongation of the PDMS substrate. Reproduced with permission.[14] Copyright 2011, Nature Publishing Group. c) Microcrack initiation and propagation on the graphene thin film–PDMS composite under stretching and microcrack recovery under releasing cycle. Reproduced with permission.[76] Copyright 2012, Nature Publishing Group.

where V is the electrical potential difference, A is the cross sectional area of the tunneling junction, J is the tunneling current density, h is Plank's constant, d is the distance between adjacent nanomaterials, e is the single electron charge, m is the mass of electron, and λ is the height of energy barrier for polymers. The cut-off tunneling distance depends on several factors such as type of conductive materials, type of insulating media, and processing parameters.[71] For example, cut-off distances of the AgNW–PDMS–AgNW and CNT–polymer–CNT channels were reported to be about 0.58 and 1–1.8 nm, respectively.[10,42,107] The tunneling cut-off distance between two parallel graphene sheets insulated with polymers was determined to be around 2–3 nm.[109,110] This value is larger than the cut-off distances for AgNWs or CNTs because of the highly crumpled nature of graphene sheets.[110] The dominant strain-responsive mechanism of the (CNTs or graphene)–polymer nanocomposites based strain sensors was discovered to be the tunneling effect.[34,35,62,71,82,90,107,108,110] Moreover, single CNT and monolayer graphene possess high tensile strength up to 40% and 30% with fully reversible structural geometry due to the energy absorption of the carbonic hexagonal honeycomb structure.[34,55,90] Therefore, CNTs and graphene could be regarded as elastic nanomaterials. The (CNTs or graphene)–polymer nanocomposites consist of numerous CNTs or graphene flakes that are entangled and folded in complex networks inside the polymer matrices. When an external strain is applied, unfolding of entangled elastic nanomaterials is more probable than sliding in their axial directions, changing the tunneling resistance. This mechanism is different from the disconnection mechanism where several connected junctions are separated due to the sliding of rigid nanomaterials inside the polymer matrices.

4. Performance of Stretchable Strain Sensors

Strain sensing performance of stretchable strain sensors has been characterized by different performance parameters such as stretchability, sensitivity or gauge factor (GF), linearity, hysteresis, response and recovery time, overshoot behavior, durability, etc. These parameters are crucial for stretchable and wearable strain sensor characterization since large, long-duration, and frequent strains may be applied to the strain sensors during such applications.

4.1. Stretchability

Stretchability of strain sensors is diverse, depending on the type of strain sensors, nanomaterials, micro/nanostructures, and even fabrication process. Highly stretchable ($\varepsilon \approx 280\%$) resistive-type sensors were reported based on the aligned CNT thin film–PDMS composites.[14] High stretchability was achieved by highly homogeneous microcrack propagation in the CNT thin film as well as lateral interconnection between aligned CNTs upon stretching. In parallel, ultra-high stretchable ($\varepsilon \approx 300\%$) capacitive-type sensors were presented by using percolating CNT network-silicone elastomer composites owning to the high stretchability of the dielectric layer and robustness of the

Adv. Funct. Mater. **2016**,
DOI: 10.1002/adfm.201504755

Table 1. Summary of performance results of recently reported stretchable strain sensors.

Reference	Type of sensor	Materials	Stretchability (%)	Gauge factor	Linearity
[10]	Resistive	AgNWs–PDMS	70	2–14	Linear up to 40%
[11]	Resistive	CNTs–Ecoflex	500	1–2.5	Linear
[12]	Resistive	CBs–PDMS	30	29.1	Linear
[14]	Resistive	Aligned CNTs–PDMS	280	0.82	Two linear regions
[29]	Resistive	ZnONWs–PDMS	50	114	Linear
[33]	Capacitive	CNTs–Dragon-skin elastomer	300	0.97	Linear
[46]	Resistive	Graphene foam–PDMS	70	15–29	Linear
[51]	Resistive	CBs–TPE	80	20	Nonlinear
[52]	Resistive	CBs–PDMS	10	1.8–5.5	Two linear regions
[53]	Capacitive	CNTs–Ecoflex	150	1	Linear
[57]	Resistive	CBs–Ecoflex	400	3.8	Nonlinear
[58]	Capacitive	CNTs–silicone elastomer	100	0.99	Linear
[61]	Resistive	Graphene–rubber	800	10–35	Nonlinear
[65]	Capacitive	AgNWs–Ecoflex	50	0.7	Linear
[70]	Resistive	Platinum (Pt)–PDMS	2	2,000	Nonlinear
[74]	Resistive	AuNWs–PANI–rubber	149.6	20.4–61.4	Linear
[75]	Resistive	AgNWs–PEDOT:PSS/PU[a)]	100	1.07–12.4	Nonlinear
[105]	Resistive	AuNWs–latex rubber	350	6.9-9.9	Linear
[131]	Resistive	CNTs–PEDOT:PSS/PU	100	8.7–62.3	Nonlinear

[a)] (PEDOT:PSS: poly(3,4-ethylenedioxythiophene) polystyrenesulfonate and PU: polyurethane).

CNT-based stretchable electrodes.[33] The stretchability of strain sensors was considerably improved by using 1D nanomaterials-polymers composites (**Table 1**).[10,29,33,59,74] As 1D nanomaterials have high aspect ratio, the effective percolation networks can be easily formed and the thin films can sustain stable electromechanical characteristics even for high strain levels. The CB, NP, and graphene thin films based strain sensors typically exhibited low stretchability ($\varepsilon \leq 10\%$),[12,36,50–52,54,55,67–70,74,76] except for the crumpled graphene-nanocellulose nanopaper composite ($\varepsilon \approx 100\%$), fragmentized graphene foam (FGF)–PDMS nanocomposites ($\varepsilon \approx 70\%$), graphene-rubber composites ($\varepsilon \approx 800\%$), and CBs–TPE nanocomposite ($\varepsilon \approx 80\%$) strain sensors where stretchability was improved by their special 3D fibrous structures (**Figure 4**a and 4b).[46,47,51,61] The low stretchability of the CBs, NPs, and graphene based strain sensors could be explained by the lack of robust percolating networks of the low aspect ratio nanomaterials.

4.2. Sensitivity or Gauge Factor (GF)

Slope of the relative change of the electrical signal, often resistance or capacitance, versus applied strain reflects GFs of strain sensors. GFs are given by GFs = $(\Delta R/R_0)/\varepsilon$ and GFs = $(\Delta C/C_0)/\varepsilon$ for resistive-type and capacitive-type sensors, respectively. Conventional metal-foil based strain gauges possess GFs in the range of 2–5 and semiconductor based strain sensors might bear GFs of 100 or larger.[10,54,90] For stretchable strain sensors, the value of GFs is diverse, depending on the piezoresistive mechanisms, nanomaterials, and micro/nanostructures of strain sensors. The CNTs–Ecoflex nanocomposite based resistive-type sensors showed GFs of 1–2.5 by the change of the tunneling resistance upon stretching.[11] The AgNWs-PDMS nanocomposite based resistive-type sensors exhibited tunable GFs in the range of 2–14.[10] GFs were controlled by number density of the AgNW percolation network. Lower density networks resulted in more effective disconnection between NW-NW junctions and thus higher GFs. Despite the enhancement of sensitivity by lowering the network density for several strain sensors,[10,11,46,54,61] the stretchability of strain sensors was considerably decreased (**Figure 5**a). Highly sensitive (GFs ≈ 116) resistive-strain sensors have been reported by using ZnONWs-polymer composites. The high GF has been achieved by the unique "nanobrush" structure (Figure 4c) as well as the growth of short ZnONWs (≈3 μm), leading to large number of disconnections between ZnONW–ZnONW junctions by the applied strain.[29] In another approach, ultra-high sensitive (GFs ≥ 1000) have been illustrated using graphene thin films-polymer composites, employing high-density microcrack generation in the crisscross configuration (Figure 3c).[76] Despite the high sensitivity of microcracks based strain sensors, they typically exhibited low stretchability ($\varepsilon \leq 30\%$).[56,70,76] Generally, stretchable strain sensors based on microcrack and disconnection mechanisms showed higher sensitivity than other piezoresistive mechanisms.[10,34,46,76] Even though capacitive-type sensors possessed high stretchability, they exhibited very low sensitivity (GF ≤ 1) due to theoretical limitations (GFs = $(\Delta C/C_0)/\varepsilon = ((1+\varepsilon)C_0 - C_0)/\varepsilon C_0 = 1$). For example, AgNW network based stretchable strain sensors with PDMS and Ecoflex dielectric layers showed GFs of 1 and 0.7, respectively.[65,83]

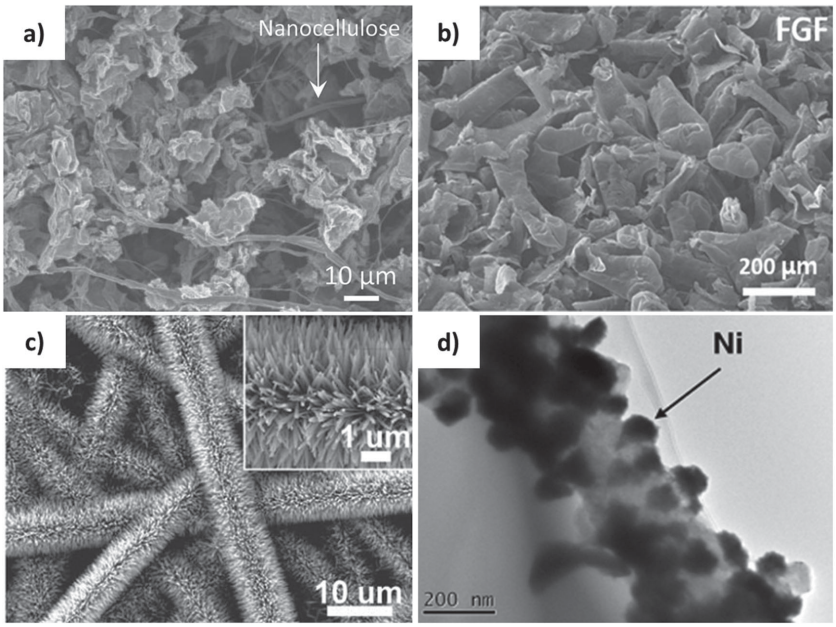

Figure 4. Hybrid nanomaterials and structures used in flexible strain sensors. a) 3D robust network of crumpled graphene and cellulose fibrils. Reproduced with permission.[47] b) 3D percolation network of FGF–PDMS nanocomposites. Reproduced with permission.[46] c) ZnONW hybrid nanobrush structures for high strain sensing; inset, high resolution microscopic image. Reproduced with permission.[29] d) Ni coated CNT hybrid structure for linear strain sensing. Reproduced with permission.[32] Copyright 2013, Elsevier.

On the other hand, GF of 0.97 was demonstrated by using CNT percolation network electrodes and Dragon-Skin dielectric layer.[33]

4.3. Linearity

Linearity is an important parameter for stretchable strain sensors because very large strains should be accommodated by strain sensors. Nonlinearity of sensors makes the calibration process complex and difficult. Nonlinearity is one of the main drawbacks of almost resistive-type strain sensors (Table 1). Generally, once the microstructure of thin films undergoes change from "homogeneous morphology" to "nonhomogeneous morphology" upon stretching, strain sensors respond to the applied strain with a nonlinear manner.[10,48] For example, inhomogeneous microcrack generation and propagation in thin films made of NPs or graphene flakes led to high nonlinear response of strain sensors (Figure 5b).[56,67,69,76,104] Furthermore, change of the "homogeneous percolation network" to the "inhomogeneous

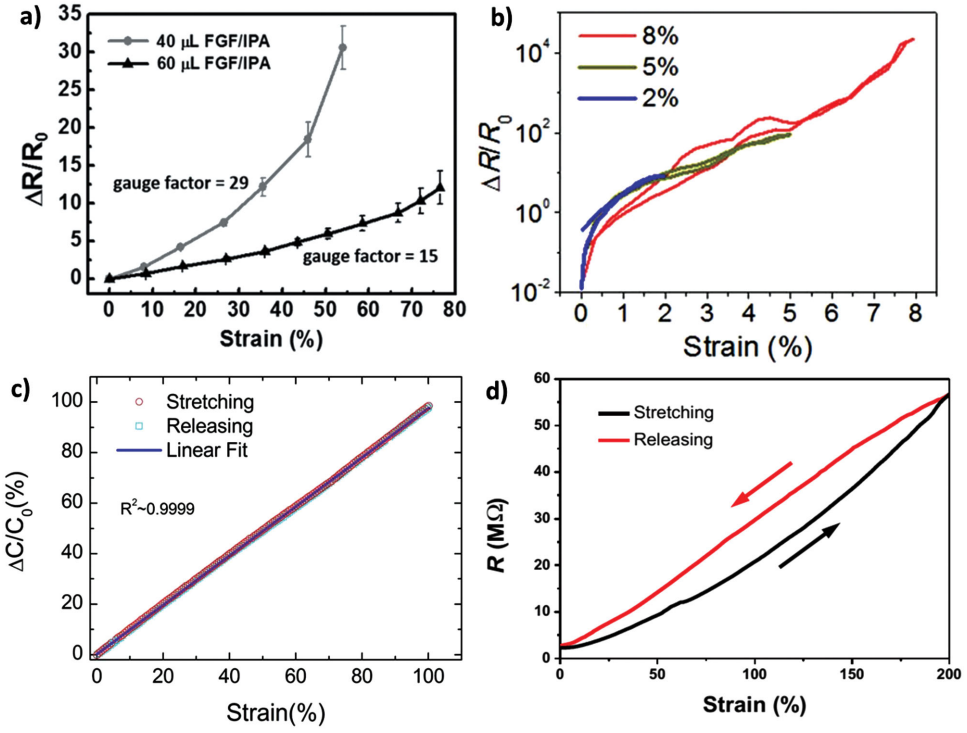

Figure 5. a) Sensitivity enhancement by lowering the density of percolation network through amount of drop-casted FGF. Reproduced with permission.[46] b) High nonlinear response of the graphene microcracked thin films upon stretching. Reproduced with permission.[76] Copyright 2012, Nature Publishing Group. c) High linear response with negligible hysteresis behavior of the CNTs–PDMS composite capacitive-type sensors. Reproduced with permission.[33] Copyright 2013, Nature Publishing Group. d) Hysteresis of the AuNWs–latex rubber composite resistive-type strain sensors. Reproduced with permission.[105] Copyright 2015, John Wiley and Sons.

DOI: 10.1002/adfm.201504755

percolation network" for the low-density AgNW network sensors was found as the main reason of nonlinearity.[10] CNTs-polymer composites based strain sensors typically exhibited nonlinear electromechanical performance with low sensitivity.[32,42,48,49,59,71,111–113] Both sensitivity and linearity of the CNTs-polymer composites were improved by their hybrid structures. For instance, metal-coated CNT-epoxy nanocomposites (GFs ≈ 155) (Figure 4d) and CNTs–graphite flake hybrid thin film coated on PET (GFs ≈ 7.8) showed high linearity and sensitivity, but with very low stretchability ($\varepsilon \leq 1.5\%$).[32,72,73,78,114] Capacitive-type sensors showed excellent linearity, but with low sensitivity (Figure 5c and **Figure 6**).[58,65] In overall, we found a trade-off relationship between "high sensitivity" and "high linearity and stretchability" in majority of strain sensors (Figure 6).[10,49,51,72] Furthermore, high sensitive strain sensors need considerable structural deformations upon stretching whereas high stretchable sensors should be morphologically intact under large stretching and both features could not be achieved through simple thin film structures. Highly sensitive strain sensors typically responded to the applied strain with high nonlinearity and low stretchability, and vice versa. Therefore, development of strain sensors with both high stretchability ($\varepsilon \geq 100\%$) and highly sensitivity (GFs ≥ 50) is still a grand challenge (Figure 6).

4.4. Hysteresis

Hysteresis becomes important when strain sensors are under dynamic load, for example, the use of sensors for skin-mountable and wearable applications. Large hysteresis behavior leads to the irreversible sensing performance of sensors upon dynamic loadings.[42,60] Capacitive-type sensors exhibited better hysteresis performance than resistive-type strain sensors (Figures 5c and 5d).[10,33,65,105] Moreover, the performance of capacitive-type strain sensors relies on the stable overlapped area between opposing electrodes, but not conductance history of electrodes. On the other hand, strain sensing of resistive-type strain sensors is highly affected by the conductance change of thin films,

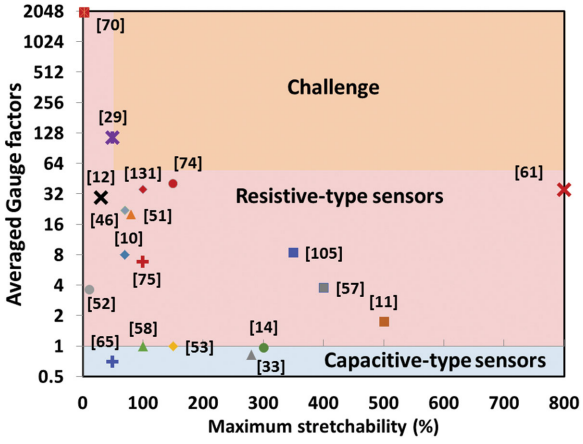

Figure 6. Averaged gauge factors as a function of maximum stretchability of recently reported resistive-type and capacitive-type strain sensors. Development of strain sensors with high stretchability, sensitivity, and linearity is still challenging (orange colored region).

causing larger hysteresis behavior. Hysteresis is mainly caused by the viscoelastic nature of polymers as well as the interaction between nanomaterial fillers and polymers.[10,42,52,59,60] Despite the negligible hysteresis for strains up to 40%, we observed high hysteresis in the response of the AgNWs–PDMS nanocomposite sensors for larger strains, caused by the hysteresis behavior of PDMS elastomer itself.[10,60,66,115] For strain sensors made of nanomaterial fillers inside polymer matrices in the form of nanocomposites, interaction between nanomaterials and polymers could be another possible reason for hysteresis. Strong interfacial binding between elastic nanomaterials (e.g., CNT and graphene) and polymers would give better strain sensing performances.[46,62,77,116] When the binding is weak, elastic nanomaterials can slide inside the polymer matrices upon high stretching while they cannot rapidly slide back to their original positions after complete release of strain, resulting in high hysteresis behavior.[46] On the contrary, very weak interfacial adhesion between rigid nanomaterials (e.g., metal NWs) and polymers is demanded for the full recovery of the nanomaterials to their initial positions upon releasing. If the interfacial binding is strong enough, friction force between rigid nanomaterials and polymers can lead to buckling and facture of nanomaterials at the releasing cycle.[10,83] Large hysteresis behavior of the CNT–polymer nanocomposite strain sensors can be explained by our proposed model since several researchers have pointed the weak interfacial binding between CNTs and polymers.[14,34,42,52,53,62,100,116] These studies highlight the importance of polymer materials and their interaction with sensing thin films in stretchable sensors for high performance strain sensing.

4.5. Response and Recovery Time

Response time determines how quickly the strain sensors move toward steady state response. Response delay exists in all polymer based strain sensors due to the viscoelastic nature of polymers.[10,105] A 90% time constant ($\tau_{90\%}$) is commonly used as the standard response time value for stretchable sensors.[10] The AgNWs–PDMS and ZnONWs–polystyrene composites based resistive-type strain sensors showed response time of 200 ms and 140 ms, respectively.[10,29] The CNTs–Ecoflex nanocomposite based resistive-type strain sensors showed response time of 332 ms. The larger response time of the CNTs–Ecoflex nanocomposite strain sensors could be due to the ultra-softness of the Ecoflex elastomer, providing lower force for the quick reestablishment of the CNT percolation network.[11] Capacitive-type strain sensors showed faster response time.[33] For example, AgNWs and CNTs based capacitive-type strain sensors possessed response time of 50 and 100 ms, respectively.[33,65] Recovery time is another important performance parameter of stretchable strain sensors under dynamic loads. Recovery time of capacitive-type sensors was reported to be in sub-second scale (100 ms for Ref. [33]), while it was noticed to be few seconds for resistive-type sensors. For the aligned CNT thin films–PDMS and CBs–elastomer composites strain sensors, as examples, the recovery time was about 5 and 100 s, respectively.[14,51] Nanocomposites based strain sensors exhibited longer recovery time due to the friction force between fillers and polymer matrices, leading to slow recovery of conductive network.[14]

4.6. Overshoot Behavior

Overshooting was reported for both resistive-type and capacitive-type stretchable sensors due to the stress relaxation of polymers.[14,33,44,57,67,111,117,118] Moreover, resistive-type sensors exhibited larger overshooting behavior than capacitive-type sensors. In fact, when the strain is suddenly reserved at the end of the stretching cycle, polymers intend to release their stress instantly by mechanical deformations.[111] Moreover, internal structures of polymers respond to the mechanical stress by molecular or molecular segment motions. These internal structural changes may not affect the permittivity of the dielectric layer considerably, causing a small overshoot behavior of capacitive-type strain sensors. On the other hand, this small deformation may change the distance between several nanomaterials and the total resistance of resistive-type strain sensors. The overshoot values are believed to be dependent on the viscoelasticity of polymers, GFs of strain sensors, and strain rate.

4.7. Dynamic Durability

Dynamic durability represents the endurance of strain sensors to the long-term stretching/releasing cycles with stable electrical functionality and mechanical integrity. Durability is more important for skin-mountable and wearable strain sensors since very large, complex, and dynamic strains should be accommodated by strain sensors. Degradation of the performance of strain sensors was reported by several researchers mainly caused by the fatigue and plastic deformation of polymer substrates under high strains and fracture and buckling of sensing nanomaterials.[10,66] However, a few stretchable strain sensors have also been reported with remarkable dynamic durability. For example, high durability of 3300 and 1800 stretching/releasing cycles for strain sensors made of the CNTs/PDMS and CNTs/Dragon rubber composites both under strain of up to ≈ 200% have been demonstrated.[14,33] The high durability of sensors was probably due to the high elastic behavior of CNTs, preventing plastic deformation and facture of CNTs under dynamic loading.

In summary, the advantages of capacitive-type sensors are obvious-they possessed high linearity, stretchability, and low hysteresis performance. However, capacitive-type sensors were suffering from very low GFs (GFs ≤ 1) (Table 1). In addition, unpredictable capacitive response due to the unstable overlaps between capacitive areas and capacitive interaction with human body are other drawbacks of capacitive-type stretchable sensors.[11,33,65] Although resistive-type strain sensors possessed high GFs, they typically responded to the applied strain with high hysteresis and nonlinearity, especially in the case of nanocomposites based strain sensors.

5. Computational Analysis

Piezoresistive mechanisms of several stretchable strain sensors are not fully understood yet due to difficulties and limitations associated with experimental setup. The main challenge, therefore, is in situ tracking of the microstructure of strain sensors under dynamic loadings. New computational models and numerical methods have thus become growing areas of interest to further discover the mechanics behind the strain-responsive behavior of strain sensors.[10,14,42,54,67,76]

We conducted a comprehensive numerical simulation on the piezoresistivity of the AgNWs–PDMS nanocomposite based stretchable strain sensors.[10,64] AgNWs were randomly assigned into the PDMS matrix to construct the 3D network model. The position and orientation of each NW were calculated by using space coordinate system. Junction identification was then investigated for all pair of NWs. Moreover, junctions between two adjacent NWs were classified as: (i) Complete connection without contact resistance, (ii) Fully disconnected NWs, and (iii) Tunneling current between neighboring NWs within a cut-off distance of 0.58 nm. The total resistance of strain sensor was then calculated by using 3D network resistor model under different strains. **Figure 7**a shows the relative change of resistance versus applied strains from 0% to 100% calculated by numerical simulation, in a great agreement with experimental results. Figure 7b illustrates the number of disconnected NWs and tunneling junctions upon stretching. The number of disconnected NWs linearly increased with the applied strain whereas tunneling junctions were very small and their piezoresistive effect were negligible. Morphological changes in the low and high density AgNW networks were also investigated by numerical analysis. Figures 7c and 7d illustrate the top projected view of the low and high density AgNW networks, respectively. As shown in Figure 7c, bottlenecks emerged in the low-density AgNW network. Bottleneck locations critically limited the electrical conductivity upon stretching, resulting in a sharp increase of the resistance with a nonlinear fashion. On the other hand, emergence of the bottlenecks was less probable in the case of the high-density network because of large number of connected NWs within the percolation network (Figure 7d). Furthermore, the change of the low-density network from "homogeneous morphology" to the "inhomogeneous morphology" induced nonlinearity in the piezoresistive response. The effect of the aspect ratio of NWs on the stretchability and linearity of strain sensors was further studied. Strain sensors made of longer NWs exhibited better linearity, but with lower sensitivity. Moreover, more NW–NW junctions contributed into the piezoresistive effect for short NW networks, resulting in higher sensitivity.[64]

The simulation of strain-responsive mechanism for stretchable strain sensors made of the overlapped graphene flakes coated on polymer layers was also reported.[54,76,104] The percolation network of the randomly orientated circular graphene flakes with uniform size distribution was analyzed.[104] **Figure 8**a shows the percolation network of the randomly assigned graphene flakes. The total resistance of the thin film was calculated by the resistor network analysis, considering resistance of graphene flakes and contact resistance among overlapped graphene flakes. Figure 8b illustrates the voltage drop across the percolation network of the graphene thin film under strain. More stretching led more increase of the contact resistance through decrease of the overlapping areas. As depicted in Figure 8c and 8d, the sensitivity of strain sensors was tuned by the control of either thickness or initial resistance of the thin

Adv. Funct. Mater. **2016**,
DOI: 10.1002/adfm.201504755

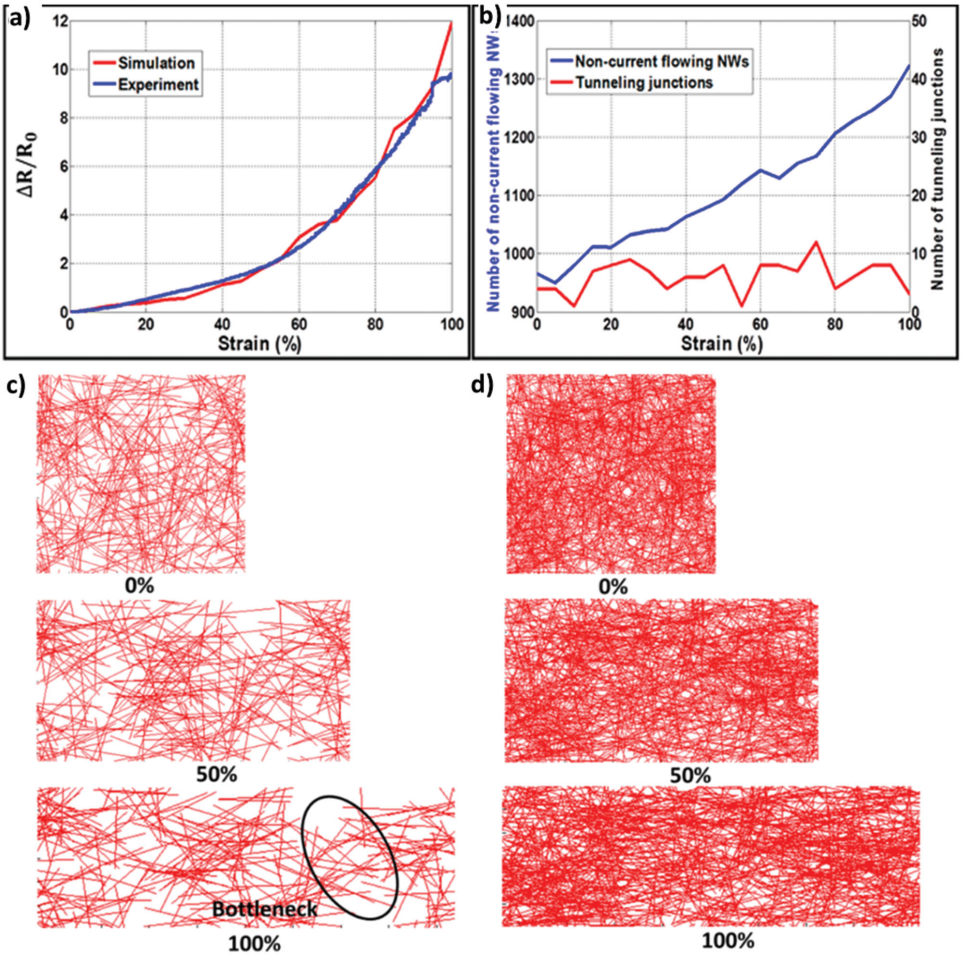

Figure 7. Simulation of the piezoresistivity of the AgNW percolating networks. a) Relative change of the resistance versus applied strain-both simulation and experiment. b) Change in the number of disconnected NWs and tunneling junctions upon stretching. c) Bottleneck locations in the case of the low-density networks. d) Change of the network morphology for the high-density network. Reproduced with permission.[10] Copyright 2014, American Chemical Society.

films. GFs increased by the thinner films due to the fewer electrical connections of the low-density network. Similarly, Hempel et al. considered the effect of the number density on the strain-responsive behavior of graphene thin films.[54] More sensitive strain sensors were achieved by the lower number density of graphene flake thin films. In the low-density percolation, few conduction clusters contributed into the electrical conductivity and reorientation of the percolation network steeply increased the electrical resistance.

Strain-responsive mechanism of the AgNP thin film patterned on the PDMS substrate was demonstrated by Lee et al.[67] AgNPs were randomly distributed on the PDMS substrate (**Figure 9**a). The adhesion in the interface of AgNP–AgNP and AgNP–PDMS was assumed as elastic bonds with maximum allowable strains, randomly assigned throughout the thin film. If the strain between AgNPs exceeded the maximum allowable strain, the cohesive force between AgNPs disappeared and breakage between NPs happened. The top projected view of the thin film stretched from 0% to 25% and then released to 0% is illustrated in Figure 9a. Under stretching, microcracks were opened and propagated throughout the thin film. More stretching created larger and longer microcracks. The resistance of the strain sensor was gradually increased by the applied strain with a nonlinear fashion (Figure 9b). Piezoresistive response of the strain sensors with pre-crack condition was also calculated (Figure 9b). Thin films with initially assigned microcracks possessed more sensitivity than that of the uniform thin film. The stress concentration near pre-cracked tips may foster larger and longer cracks, resulting in larger resistance change in the pre-cracked thin films.

Conductivity and piezoresistivity of CNTs–polymer nanocomposites were computationally studied by considering CNTs as rigid capped cylinders with zero contact resistance in CNT–CNT junctions. Neglecting the intrinsic piezoresistivity of CNTs, elastic behavior of individual CNT as well as deformation of CNT walls transversely in the CNT–CNT junctions overestimated the overall conductance and piezoresistive behavior of CNTs–polymer nanocomposites.[35,112,119,120] Recently, the validation of simulation results was remarkably improved by considering the deformation of CNT walls in the contact areas.[112,121] It was demonstrated that the increase of the contact resistance due to the increase of the intrinsic resistance

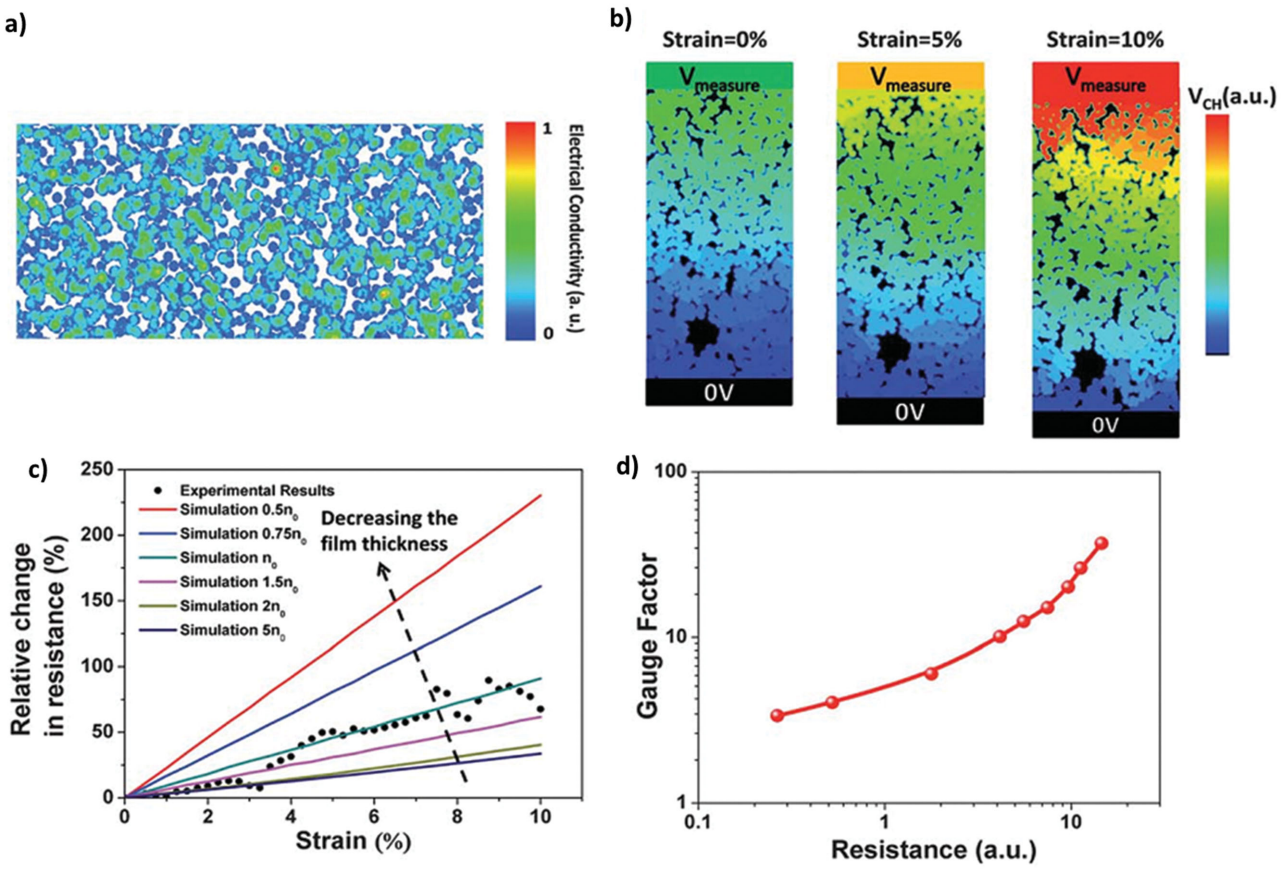

Figure 8. Computational analysis of the graphene thin film strain sensors. a) Percolation network of the randomly assigned graphene flakes. b) Voltage drop in the two ends of the graphene thin film upon stretching due to the decrease of the overlapped area. c) The effect of the thin film thickness on the piezoresistivity of the graphene thin films. d) Enhancement of sensitivity by increasing the base resistance of the graphene thin film based strain sensors. Reproduced with permission.[104] Copyright 2013, Royal Society of Chemistry.

of CNT cause by the wall deformation is significant. Simulations indicated that the tunneling resistance change is the main mechanism of the piezoresistivity of CNTs–polymer nanocomposite strain sensors.[107,108,110,112] The nonlinearity of CNTs–polymer nanocomposite strain sensors was referred to the nonlinear tunneling effect. Moreover, the effects of parameters such as size, shape, tunneling area, and height of barrier on the piezoresistivity of the CNTs–polymer nanocomposites were extensively studied.[42,108,112,119] However, all abovementioned papers explored the piezoresistivity of the CNTs–polymer nanocomposites under small strains ($\varepsilon \leq 1\%$).[35,42,107,122] Strain-responsive behavior of CNTs–polymer nanocomposites at larger strains needs further investigations.

Electrical transport in graphene flakes dispersed in polymers in the form of nanocomposites was also investigated by using tunneling percolation and Monte Carlo simulations.[109,110] Oskouyi et al. investigated the strain-responsive behavior of graphene–polymer nanocomposites considering several factors such as size and aspect ratio of graphene flakes, electrical properties of polymers, and different tunneling cut-off distances.[109] It was demonstrated that volume fraction of conductive fillers plays an important role in the piezoresistivity of the graphene–polymer nanocomposites. However, elastic behavior of graphene flakes inside polymer matrices, intrinsic piezoresistivity of graphene flakes, and crumpled and wrinkled nature of graphene flakes were neglected in all previously reported papers.

6. Applications

There are numerous potential applications for flexible strain sensors. For example, low-strain gauges can be implemented for the structural health-monitoring,[123,124] mass measurement,[125,126] pressure sensing,[67,81] etc. On the other hand, highly stretchable and sensitive strain sensors could be utilized as body-integrated electronic devices. They can be attached onto the clothing or directly laminated on the human skin for the body strain measurement, ranging from minute skin motions induced by respiration and heartbeat to human body large strains like bending/straightening of body joints. In addition, soft strain sensors would be beneficial for the strain measurement in soft-bodied robots.

6.1. Biomedical Applications

Health-care and good quality medication are becoming very complex and difficult due to the raise in the population. Remote and personalized health-monitoring are promising

DOI: 10.1002/adfm.201504755

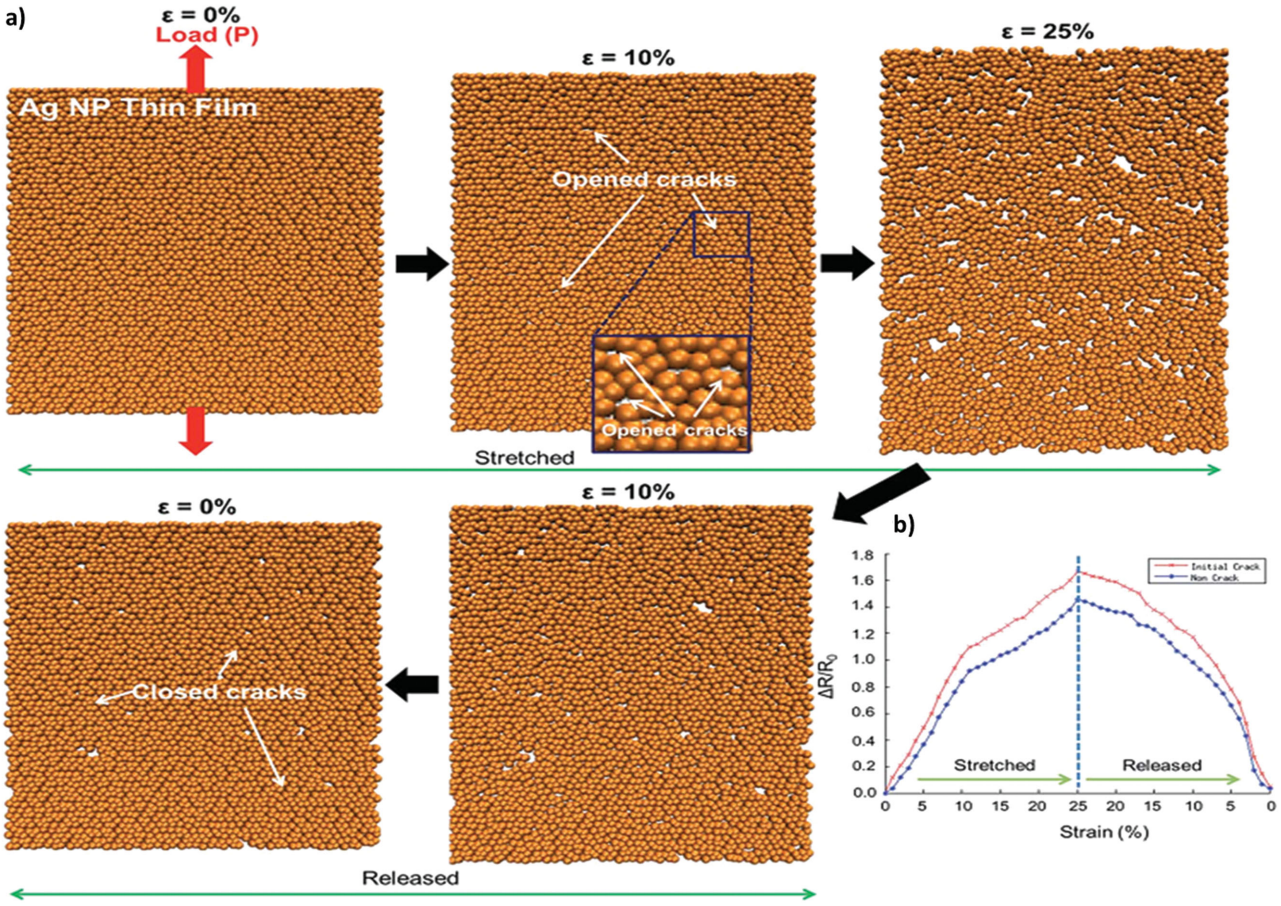

Figure 9. Computational analysis of the AgNP thin film strain sensors. a) Morphological changes in the microstructure of the AgNP thin film under stretching and releasing; microcrack opening propagation upon stretching. b) Relative change of the resistance versus applied strain for AgNP thin films with and without pre-crack conditions. Reproduced with permission.[67] Copyright 2014, Royal Society of Chemistry.

solutions to expand the capability of current medical systems, extend the health-care range into the community, and improve the diagnosis and early treatments.[38,127,128] Nowadays, high attention is directed to wearable technologies owning to their easy implementation, early diagnosis, and long-term monitoring capabilities.[1,7,127,128] **Figure 10** shows the conceptual representation of the remote and personalized health-monitoring by the use of wearable sensors.[127] Wearable sensors gather physiological and environmental data from human body in a natural way. Measured data could be blood pressure and oxygen saturation,[4,128] breathing rate,[14,16,56,106] heartbeat,[5,56] human body temperature,[2,21] movements,[10,12,14] and beyond. Wireless or internet communications could be used to transmit the measured data from wearable sensors to a mobile phone or an access point and alter a medical center. For emergency situations, an alarm message is sent to an emergency service center to provide immediate assistance. After sufficient medical treatment, health-care professionals can remotely monitor patient's status and make medical decisions.[127,128]

Among wearable sensors, stretchable strain sensors can potentially function for several biomedical applications. Such sensors should be highly stretchable and flexible to mimic complex and large deformations of the human skin or clothing and sufficiently possess high sensitivity to be able to detect minute skin strains induced by blood flow pulse or respiration. **Figure 11**a shows in vitro blood pressure monitoring using a flexible capacitive-type sensor. The sensor was wrapped around the carotid artery of a pig and diameter changes of the vessel due to the blood flow pressure were measured. The designed sensor showed fast response time (50 ms) and sensitivity (0.045% mmHg) for the blood pressures in the range of 0–200 mmHg.[4] The sensor responded to the dynamic blood pressure with a good strain sensing performance and measured pressure ranges were well-matched with the real data (Figure 11b). In another approach, highly sensitive, skin-mountable, and wearable strain sensors have been developed for the tiny skin motion detection induced by phonation, facial expression, tissue swelling, wound healing, breathing, and pulse.[12,56,75,105] Inset of Figure 11c illustrates a resistive-type sensor fixed to the chest area. The response of the sensor to the breathing both in still (black) and movement (red) sates is depicted in Figure 11c. Peaks and valleys represent the stretching and shrinkage of the chest upon respiration, respectively. Heartbeat measurement of the sensor while attached to the wrist is shown in Figure 11d. The pulse numbers in still (black) and exercise (red) states were 38 and 46 in 30 s, respectively, which both are within the normal range of a healthy person.[56] Long-term monitoring of blood flow pulse

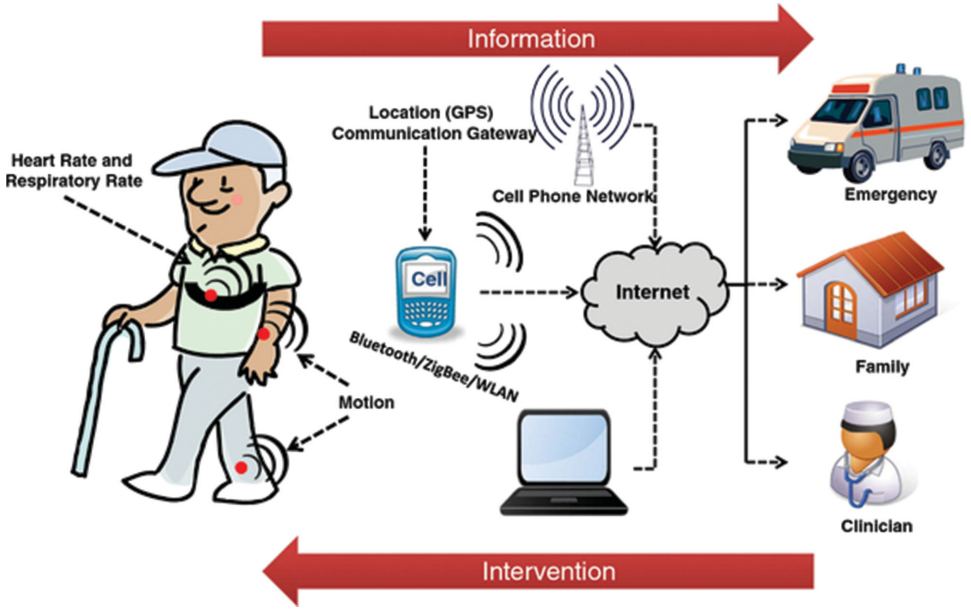

Figure 10. A conceptual schematic of remote and personalized health-care systems; collection of patients' physiological information by wearable sensors and then transmission of sensors' data to a medical center via wireless networks or internet; alerting emergency center, medical doctors, and family members in the case of emergency situation for medical assistant. Reproduced with permission.[127] Copyright 2012, BioMed Central.

and respiration rate, as vital signs, can be potentially employed for the personalized health-monitoring and early diagnosis of diseases. Patellar reflex test was conducted by using a stretchable capacitive-type sensor.[65] The sensor was attached onto the knee while the person was sat with naturally relaxed leg (Figure 11e). At this state, a large strain was accommodated by the sensor since the knee was fully bent. To test the patellar reflex, a hammer was used to tap the patellar tendon ligament. As a normal response, the leg should straighten and then come to its initial position quickly. Figure 11f clearly indicates that the capacitance of the sensor was decreased suddenly and then returned to its initial value. Overall, there are several biomedical applications for skin-mountable and wearable strain sensors. Resistive-type sensors would be beneficial for low-strain motions due to their high sensitivities while capacitive-type sensors show better performances in terms of linearity, low hysteresis, and fast response for high-strain motions.

6.2. Sports Performance Monitoring

Skin-mountable and wearable strain sensors can function for the sport performance monitoring by mounting them in different parts of the body. **Figures 12**a and 12b show the output signal of skin-mountable strain sensors attached to the wrist and elbow.[11] The resistance of strain sensors increased upon bending of wrist and elbow and then recovered to its original value after straightening them. The sensory information can be used for the body movement analysis during sport activities. Figure 12c illustrates a rosette-type stretchable strain sensors made of three independent CBs-PDMS nanocomposite strain sensors (e.g., S_1, S_2, and S_3) with 120° of each other.[52] Rosette-type strain sensors are capable of measuring the principle strains and their directions under in-plane deformations.[11,52,53] Figure 12d shows the response of the rosette-type sensor when it was uniaxially stretched in the direction of S_1. As shown in the figure, the change of resistance for the S_1 was larger than that of S_2 and S_3 due to the direction of stretching. The data could be potentially used for the tissue swelling and expansion monitoring during sport performances for the body fitness or wellness analysis.[11,12,52,55,128] As another application, stretchable strain sensors were mounted on the knee joint and different knee motion patterns such as walking, running, and jumping from squatting were monitored (Figure 12e).[14,65] Skin-mountable and wearable strain sensors, therefore, are beneficial for the continuous health and wellness monitoring, human-friendly rehabilitation, and evaluation of athletes' sport performances.[14,61,65]

6.3. Human-Machine Interfaces, Soft Robotics, and Haptics

The major goal of current technologies is to build smart human-machine interfaces, and one can achieve this by the use of wearable sensory systems. The signals from wearable strain sensors can be utilized to actuate smart robots. For instance, various smart gloves were developed using stretchable, skin-mountable, and wearable strain sensors.[10,14,33,57] The strain sensors were attached to the fingers of gloves for the bending angle measurement of finger joints (**Figure 13**a). When a finger joint was bent, the bending strain was accommodated by the strain sensors, causing change in the electrical signal (Figure 13b). When the finger was straightened, the strain sensor relaxed and the strain was decreased, accompanied by recovery of electrical signal (Figure 13a).[10,33,47,65] Figure 13c illustrates the remote control of a gripper robot by wearable strain sensors. The information of sensors was wirelessly transferred from smart glove to the gripper robot.

Adv. Funct. Mater. **2016**,
DOI: 10.1002/adfm.201504755

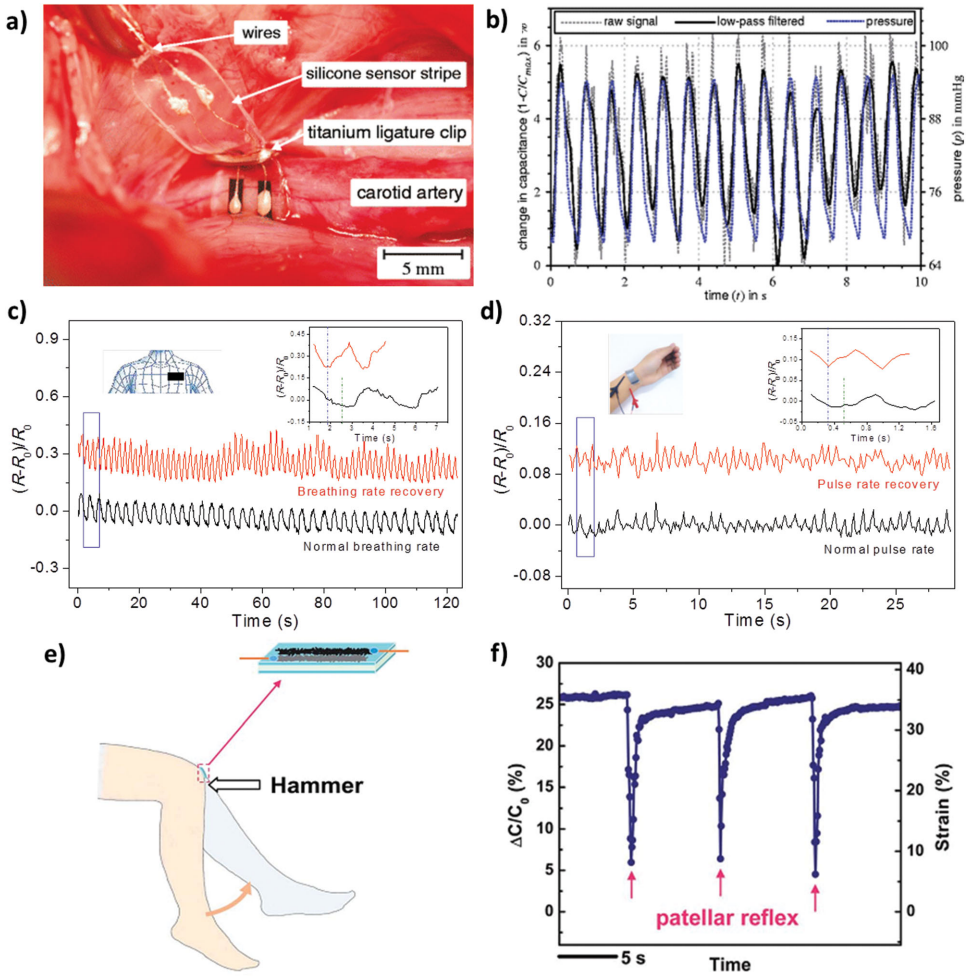

Figure 11. Biomedical applications of wearable and skin-mountable strain sensors: a) A capacitive-type strain sensor wrapped around the carotid artery of a pig. Reproduced with permission.[4] Copyright 2012, Springer. b) In vitro measurement of the blood pressure by response of the sensors to diameter changes of the vessel due to the blood flow pressure. Reproduced with permission.[4] Copyright 2012, Springer. c) Breathing monitoring by attaching a wearable strain sensor in the chest; inset, location of attached strain sensor. Reproduced with permission.[56] Copyright 2014, John Wiley and Sons. d) Blood flow pulse monitoring by mounting a wearable sensor on the wrist; inset, the strain sensor mounted on the wrist. Reproduced with permission.[56] Copyright 2014, John Wiley and Sons. e) Schematic of the patellar reflex test; a capacitive-type sensor is mounted on the knee for the strain measurement. Reproduced with permission.[65] Copyright 2013, Royal Society of Chemistry. f) Response from a strain sensor during the patellar reflex test. Reproduced with permission.[65] Copyright 2013, Royal Society of Chemistry.

Bending/straightening of fingers was utilized to control the robot for performing different tasks.[74] Remote control of slave robots by smart glove systems would be beneficial in performing surgical procedures or delicate and dangerous works that may be out of reach for the human body.[10,14,33,47] Smart glove systems developed by wearable sensors are advantageous over conventional systems based on the optical fibers and metal-strain gauges (cyber glove) in terms of high-strain sensing capabilities, fabrication cost, and simplicity.[55,76] Flexible and soft strain sensors would also be useful in soft-bodied robots for providing input to the feedback controllers as well as sensory artificial skins, allowing soft robots to sense the environment and interact with surrounding objects.[30,31] A sensory array of strain sensors can serve as artificial skins of robots for haptic perception and surface strain distribution mapping.[46,70,113] Figure 13d depicts a flexible artificial skin made of 8 × 8 arrays of strain sensors.[70] The artificial skin was able to sense both static and dynamic pressures by placing a piece of PDMS and a flapping ladybird on top of the sensory array, respectively (Figure 13e).

6.4. Virtual Reality and Entertainment Technology

As another potential impact, skin-mountable and wearable strain sensors can be utilized as motion sensors and input gears for virtual reality and interactive gaming. **Figure 14**a depicts posture-driven gaming by wearable motion sensors attached to the human body. Since the movement of the human body is required for posture-driven gaming, wearable sensors can also be used for medical training, home-rehabilitation, and therapy applications.[127] Figure 14b illustrates an

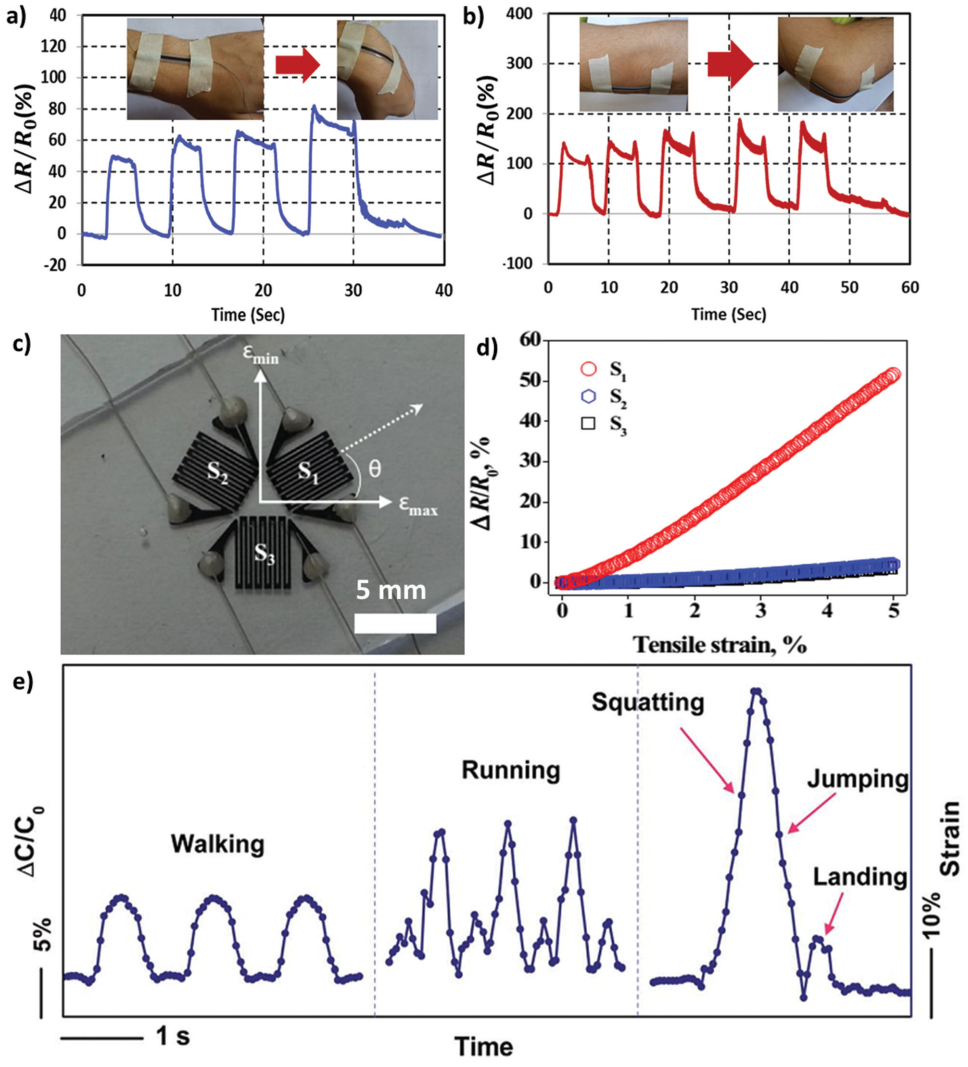

Figure 12. Applications of wearable and skin-mountable strain sensors for sport performance monitoring. a, b) Response of skin-mountable strain sensors to bending/straightening of the wrist and elbow joints; insets, photograph of the strain sensors attached onto the wrist and elbow joints. Reproduced with permission.[11] Copyright 2015, IOP Publishing Group. c) Photograph of the rosette-type strain sensor made of patterned CBs–PDMS nanocomposites. Reproduced with permission.[52] Copyright 2014, Elsevier. b) Measured signals from sensors when the rosette-type sensor was stretched in the direction of S_1. Reproduced with permission.[52] Copyright 2014, Elsevier. c) Response of a capacitive-type sensor to the different human motion patterns (e.g., walking, running and jumping from squatting) when the sensor was mounted on the knee joint. Reproduced with permission.[65] Copyright 2013, Royal Society of Chemistry.

integrated smart glove system made of five wearable strain sensors and custom-made data acquisition (DAQ) chip. An avatar was successfully controlled in the virtual environment by output signals of strain sensors.[10] This approach has several advantages over the vision-based activity recognition (motion detection by set of cameras and image processing) in terms of mobility, space requirement, cost, and resolution.[64,129–131]

7. Current Challenges

As discussed above, achievement of strain sensors with both high stretchability and high sensitivity is still a grand challenge, especially, for personalized health-care applications where highly sensitive and soft sensors are required. Although there have been some efforts to achieve unidirectional and rosette-configuration sensors,[11,44,52,113] strain sensor architectures capable of measuring decoupled strains in multi-directions and multi-plane deformations for large sensory array applications (e.g., robot skin sensors) have not been reported yet. Furthermore, strain and pressure sensitivities are coupled in many reported strain sensors.[65,103,132] Therefore, new material approaches and micro/nanostructure designs are required to enable decoupled strain and pressure sensing for flexible sensors.[132]

Another significant challenge is packaging of flexible sensors with power, signal conditioning, communication, and

DOI: 10.1002/adfm.201504755

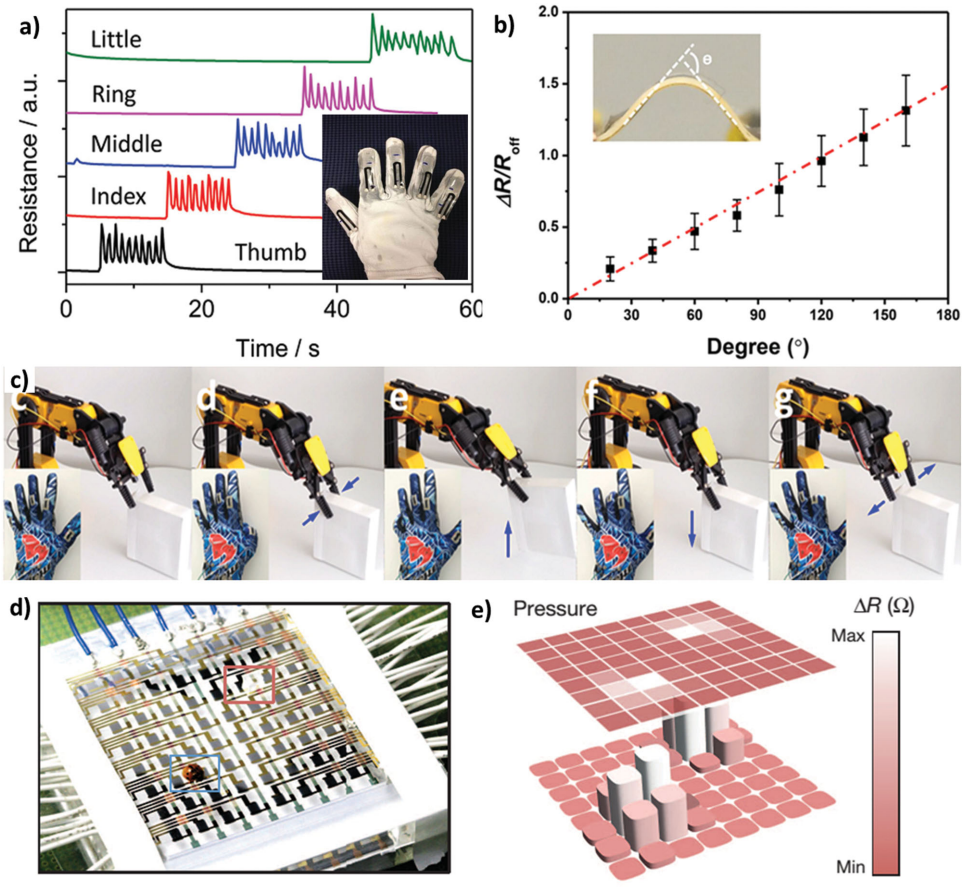

Figure 13. Robotic applications of flexible strain sensors. a) Response of wearable strain sensors to the bending/straightening of finger joints; inset, a smart glove system made of five stretchable strain sensors attached to the finger joints. Reproduced with permission.[47] b) Response of a strain sensor to the bending (resistance change versus bending angle). Reproduced with permission.[74] Copyright 2015, American Chemical Society. c) Remote control of a gripper robot by the use of a smart glove system. Reproduced with permission.[74] Copyright 2015, American Chemical Society. d) Artificial electronic skin made of 8 × 8 arrays of flexible strain sensors. Reproduced with permission.[70] Copyright 2014, Nature Publishing Group. e) Response of the artificial skin to a piece of PDMS and a flapping ladybird placed on the top of the skin. Reproduced with permission.[70] Copyright 2014, Nature Publishing Group.

data management units. To date, several approaches have been utilized for data measurement of flexible sensors. In majority of works, the sensor response was measured by conventional data acquisition systems through rigid wiring of flexible sensors with deformable interconnections (e.g., stretchable electrodes with buckled structures or serpentine-shapes, liquid metals, and non-brittle conductive pastes) (**Figures 15**a and 15b).[12,46,89,113,133,134] Moreover, most of the efforts were devoted in the sensing performance improvement rather than addressing the sensor packaging and integration. Some

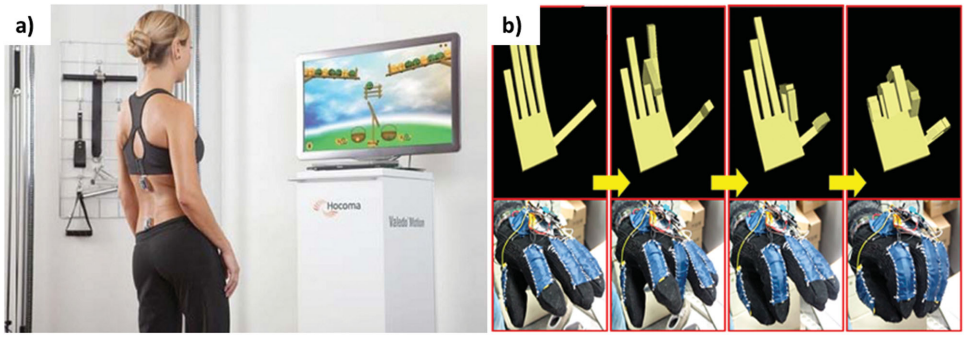

Figure 14. a) Posture-driven gaming by wearable motion sensors attached to the body. Reproduced with permission.[127] Copyright 2012, BioMed Central. b) Control of an avatar in the virtual environment by a smart glove made of five wearable strain sensors. Reproduced with permission.[10] Copyright 2014, American Chemical Society.

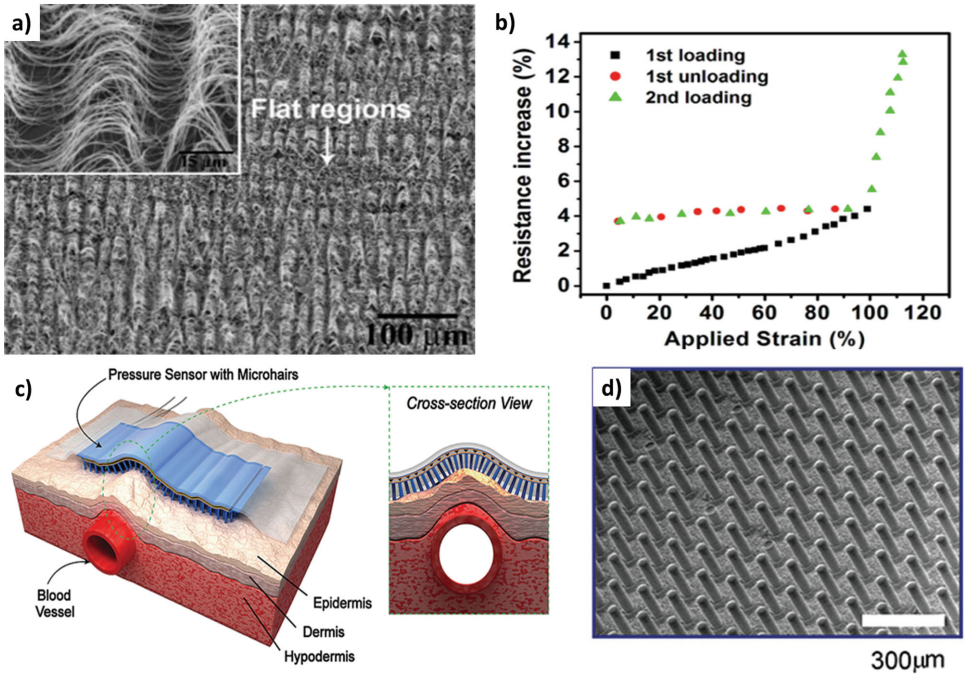

Figure 15. a) Scanning electron microscope (SEM) image of a buckled CNT ribbon induced by releasing the pre-strain of PDMS for high performance electrode applications; inset, the high magnification image. Reproduced with permission.[134] b) Resistance of a CNT ribbon–PDMS composite film as a function of tensile strain; stabilization of the resistance after first stretch/release cycle. Reproduced with permission.[134] c) Conformal attachment of skin-mountable sensors to the human skin by the use of microhair structured adhesive layers. Reproduced with permission.[15] d) SEM image of the microhair structure arrays. Reproduced with permission.[15]

papers reported custom-made data management boards made of commercial rigid electronic circuits as mobile platforms that can be integrated with flexible sensors.[10,135] However, the size of these boards is typically not small (in cm scale) and integration of such rigid elements with soft sensors seems impractical. Recently, soft microfluidic assembly of commercial and chip-scale components (e.g., sensors, circuits, and radios) was demonstrated to be promising for body-integrated applications.[136] But, the fabrication of such system is complex and time-consuming and its long-term applicability is not proved yet. In another approach, flexible energy storage and communication modules that could be directly assembled with flexible sensors have recently been reported.[137–141] However, the integration of all sensor, power, and communication modules in a soft and compact device with high reliability, robustness, and long-term monitoring capability has not been achieved yet.[22] Further investigations are needed for solving such challenge.

Conformal attachment of strain sensors on the human body is another important consideration for the highly efficient body strain measurements. Weak adhesion can lead to sliding of sensors from skin, inducing noise in the response of strain sensors and underestimating the actual strain. To avoid this problem, strain sensors can be attached onto the human skin with the aid of intermediate adhesive layers,[13–15,56,128] microhair adhesive structures[142–145] as an example, ensuring conformal contact (Figure 15c and 15d) or design of strain sensors with equal or greater mechanical compliance than that of the human skin. For example, soft elastomers like Ecoflex with Young's modulus of 125 kPa keep same stiffness as that of the human skin (Young's modulus of 25–220 kPa).[146–148]

8. Conclusions

We presented a comprehensive review on the recent technological advances of stretchable, skin-mountable, and wearable strain sensors. To understand the physical phenomenon behind the strain-responsive mechanisms of strain sensors in microstructural view, recent outcomes of several papers in this field were categorized. We found that unlike conventional strategies, several new approaches such as disconnection between overlapped nanomaterials, crack propagation in thin films, and tunneling effect have been persuaded to develop high performance stretchable strain sensors. We then compared the performance parameters of stretchable strain sensors and discussed their dynamic characteristics. Appropriate selection of functional nanomaterials and flexible substrates can yield significant improvement in the dynamic performance of strain sensors. Capacitive-type sensors offer excellent stretchability, linearity, and hysteresis performance while their sensitivity is very low. On the other hand, resistive-type sensors possess higher sensitivity and stretchability, but with hysteresis and nonlinear behaviors. We believe that stretchable strain sensors can potentially function for many applications such as biomedicine, robotics, and entertainment technology. However, challenges such as a certain degree of hysteresis, high dynamic responses with low overshoot and decay, robust and flexible

Adv. Funct. Mater. 2016,
DOI: 10.1002/adfm.201504755

packaging, and conformal attachment to the human body have to be overcome.

Acknowledgement

This work was partially supported by Fundamental Research Program (PNK4151) of the Korean Institute of Materials Science (KIMS) and National Research Foundation of Korea (NRF) (Grant No. 2015R1A5A1037668) funded by the Korean Government (MSIP).

Received: November 5, 2015
Revised: November 16, 2015
Published online:

[1] J. R. Windmiller, J. Wang, *Electroanalysis* **2013**, *25*, 29.
[2] R. C. Webb, A. P. Bonifas, A. Behnaz, Y. Zhang, K. J. Yu, H. Cheng, M. Shi, Z. Bian, Z. Liu, Y.-S. Kim, *Nat. Mater.* **2013**, *12*, 938.
[3] X. Wang, Y. Gu, Z. Xiong, Z. Cui, T. Zhang, *Adv. Mater.* **2014**, *26*, 1336.
[4] P. Bingger, M. Zens, P. Woias, *Biomed. Microdevices* **2012**, *14*, 573.
[5] C. Pang, G.-Y. Lee, T.-i. Kim, S. M. Kim, H. N. Kim, S.-H. Ahn, K.-Y. Suh, *Nat. Mater.* **2012**, *11*, 795.
[6] D.-H. Kim, R. Ghaffari, N. Lu, J. A. Rogers, *Annu. Rev. Biomed. Eng.* **2012**, *14*, 113.
[7] A. Pantelopoulos, N. G. Bourbakis, *Systems, Man, and Cybernetics, Part C: Applications and Reviews IEEE Transactions on* **2010**, *40*, 1.
[8] W. Zeng, L. Shu, Q. Li, S. Chen, F. Wang, X. M. Tao, *Adv. Mater.* **2014**, *26*, 5310.
[9] K. Takei, W. Honda, S. Harada, T. Arie, S. Akita, *Adv. Healthcare Mater.* **2014**, *4*, 487.
[10] M. Amjadi, A. Pichitpajongkit, S. Lee, S. Ryu, I. Park, *ACS Nano* **2014**, *8*, 5154.
[11] M. Amjadi, Y. J. Yoon, I. Park, *Nanotechnology* **2015**, *26*, 375501.
[12] N. Lu, C. Lu, S. Yang, J. Rogers, *Adv. Funct. Mater.* **2012**, *22*, 4044.
[13] C. Pang, C. Lee, K. Y. Suh, *J. Appl. Polym. Sci.* **2013**, *130*, 1429.
[14] T. Yamada, Y. Hayamizu, Y. Yamamoto, Y. Yomogida, A. Izadi-Najafabadi, D. N. Futaba, K. Hata, *Nat. Nanotechnol.* **2011**, *6*, 296.
[15] C. Pang, J. H. Koo, A. Nguyen, J. M. Caves, M. G. Kim, A. Chortos, K. Kim, P. J. Wang, J. B. H. Tok, Z. Bao, *Adv. Mater.* **2015**, *27*, 634.
[16] S. Gong, W. Schwalb, Y. Wang, Y. Chen, Y. Tang, J. Si, B. Shirinzadeh, W. Cheng, *Nat. Commun.* **2014**, *5*, 3132.
[17] C. L. Choong, M. B. Shim, B. S. Lee, S. Jeon, D. S. Ko, T. H. Kang, J. Bae, S. H. Lee, K. E. Byun, J. Im, *Adv. Mater.* **2014**, *26*, 3451.
[18] K. Takei, T. Takahashi, J. C. Ho, H. Ko, A. G. Gillies, P. W. Leu, R. S. Fearing, A. Javey, *Nat. Mater.* **2010**, *9*, 821.
[19] C. Wang, D. Hwang, Z. Yu, K. Takei, J. Park, T. Chen, B. Ma, A. Javey, *Nat. Mater.* **2013**, *12*, 899.
[20] S. Park, H. Kim, M. Vosgueritchian, S. Cheon, H. Kim, J. H. Koo, T. R. Kim, S. Lee, G. Schwartz, H. Chang, *Adv. Mater.* **2014**, *26*, 7324.
[21] S. Harada, K. Kanao, Y. Yamamoto, T. Arie, S. Akita, K. Takei, *ACS nano* **2014**, *8*, 12851.
[22] W. Honda, S. Harada, T. Arie, S. Akita, K. Takei, *Adv. Funct. Mater.* **2014**, *24*, 3299.
[23] C.-X. Liu, J.-W. Choi, *Eng. Med. Biol. Soc., 2009, 31st Annu. Int. Conf. IEEE*, IEEE, Picastaway, NJ, USA **2009**, 6391.
[24] T. Giorgino, P. Tormene, F. Lorussi, D. De Rossi, S. Quaglini, *Neural Systems and Rehabilitation Engineering, IEEE Transactions on* **2009**, *17*, 409.
[25] F. Lorussi, E. P. Scilingo, M. Tesconi, A. Tognetti, D. De Rossi, *Information Technology in Biomedicine, IEEE Transactions on* **2005**, *9*, 372.
[26] R. Helmer, D. Farrow, K. Ball, E. Phillips, A. Farouil, I. Blanchonette, *Procedia Eng.* **2011**, *13*, 513.
[27] C.-X. Liu, J.-W. Choi, *J. Micromech. Microeng.* **2009**, *19*, 085019.
[28] S. S. Rautaray, A. Agrawal, *2011 Int. Conf. Multimedia, Signal Processing Commun. Technol. (IMPACT)*, IEEE, Picastawa, NJ, USA **2011**, p 244.
[29] X. Xiao, L. Yuan, J. Zhong, T. Ding, Y. Liu, Z. Cai, Y. Rong, H. Han, J. Zhou, Z. L. Wang, *Adv. Mater.* **2011**, *23*, 5440.
[30] M. McEvoy, N. Correll, *Science* **2015**, *347*, 1261689.
[31] C. Majidi, *Soft Robotics* **2014**, *1*, 5.
[32] N. Hu, T. Itoi, T. Akagi, T. Kojima, J. Xue, C. Yan, S. Atobe, H. Fukunaga, W. Yuan, H. Ning, *Carbon* **2013**, *51*, 202.
[33] L. Cai, L. Song, P. Luan, Q. Zhang, N. Zhang, Q. Gao, D. Zhao, X. Zhang, M. Tu, F. Yang, *Sci. Rep.* **2013**, *3*, 3048
[34] W. Obitayo, T. Liu, *J. Sens.* **2012**, *2012*, 652438.
[35] N. Hu, Y. Karube, C. Yan, Z. Masuda, H. Fukunaga, *Acta Mater.* **2008**, *56*, 2929.
[36] J. Park, I. You, S. Shin, U. Jeong, *ChemPhysChem* **2015**, *16*, 1155.
[37] A. Frutiger, J. T. Muth, D. M. Vogt, Y. Mengüç, A. Campo, A. D. Valentine, C. J. Walsh, J. A. Lewis, *Adv. Mater.* **2015**, *27*, 2440.
[38] J. Zhong, Y. Zhang, Q. Zhong, Q. Hu, B. Hu, Z. L. Wang, J. Zhou, *ACS nano* **2014**, *8*, 6273.
[39] A. Fassler, C. Majidi, *Smart Mater. Struct.* **2013**, *22*, 055023.
[40] S. Liehr, P. Lenke, M. Wendt, K. Krebber, M. Seeger, E. Thiele, H. Metschies, B. Gebreselassie, J. Munich, *IEEE Sens. J.* **2009**, *9*, 1330.
[41] A. P. A. Raju, A. Lewis, B. Derby, R. J. Young, I. A. Kinloch, R. Zan, K. S. Novoselov, *Adv. Funct. Mater.* **2014**, *24*, 2865.
[42] N. Hu, H. Fukunaga, S. Atobe, Y. Liu, J. Li, *Sensors* **2011**, *11*, 10691.
[43] M. Rosenberger, S. Hessler, S. Belle, B. Schmauss, R. Hellmann, *Opt. Express* **2014**, *22*, 5483.
[44] R. Rahimi, M. Ochoa, W. Yu, B. Ziaie, *ACS Appl. Mater. Interfaces* **2015**, *7*, 4463.
[45] J. Rantala, J. Hännikäinen, J. Vanhala, *Personal and Ubiquitous Computing* **2011**, *15*, 85.
[46] Y. R. Jeong, H. Park, S. W. Jin, S. Y. Hong, S. S. Lee, J. S. Ha, *Adv. Funct. Mater.* **2015**, *25*, 4228.
[47] C. Yan, J. Wang, W. Kang, M. Cui, X. Wang, C. Y. Foo, K. J. Chee, P. S. Lee, *Adv. Mater.* **2013**, *26*, 2022.
[48] S. Tadakaluru, W. Thongsuwan, P. Singjai, *Sensors* **2014**, *14*, 868.
[49] S. Luo, T. Liu, *Carbon* **2013**, *59*, 315.
[50] Y. Wang, R. Yang, Z. Shi, L. Zhang, D. Shi, E. Wang, G. Zhang, *Acs Nano* **2011**, *5*, 3645.
[51] C. Mattmann, F. Clemens, G. Tröster, *Sensors* **2008**, *8*, 3719.
[52] J.-H. Kong, N.-S. Jang, S.-H. Kim, J.-M. Kim, *Carbon* **2014**, *77*, 199.
[53] U.-H. Shin, D.-W. Jeong, S.-M. Park, S.-H. Kim, H. W. Lee, J.-M. Kim, *Carbon* **2014**, *80*, 396.
[54] M. Hempel, D. Nezich, J. Kong, M. Hofmann, *Nano Lett.* **2012**, *12*, 5714.
[55] S.-H. Bae, Y. Lee, B. K. Sharma, H.-J. Lee, J.-H. Kim, J.-H. Ahn, *Carbon* **2013**, *51*, 236.
[56] Y. Wang, L. Wang, T. Yang, X. Li, X. Zang, M. Zhu, K. Wang, D. Wu, H. Zhu, *Adv. Funct. Mater.* **2014**, *24*, 4666.
[57] J. T. Muth, D. M. Vogt, R. L. Truby, Y. Mengüç, D. B. Kolesky, R. J. Wood, J. A. Lewis, *Adv. Mater.* **2014**, *26*, 6307.
[58] D. J. Cohen, D. Mitra, K. Peterson, M. M. Maharbiz, *Nano Lett.* **2012**, *12*, 1821.
[59] Q. Fan, Z. Qin, S. Gao, Y. Wu, J. Pionteck, E. Mäder, M. Zhu, *Carbon* **2012**, *50*, 4085.
[60] C.-X. Liu, J.-W. Choi, *Microelectron. Eng.* **2014**, *117*, 1.
[61] C. S. Boland, U. Khan, C. Backes, A. O'Neill, J. McCauley, S. Duane, R. Shanker, Y. Liu, I. Jurewicz, A. B. Dalton, *ACS Nano* **2014**, *8*, 8819.
[62] L. Lin, S. Liu, Q. Zhang, X. Li, M. Ji, H. Deng, Q. Fu, *ACS Appl. Mater. Interfaces* **2013**, *5*, 5815.
[63] J. J. Park, W. J. Hyun, S. C. Mun, Y. T. Park, O. O. Park, *ACS Appl. Mater. Interfaces* **2015**, *7*, 6317.

[64] M. Amjadi, A. Pichitpajongkit, S. Ryu, I. Park, *2014 IEEE 27th Int. Conf. Micro Electro Mech. Syst. (MEMS)*, IEEE, Picastaway, NJ, USA **2014**, 785.
[65] S. Yao, Y. Zhu, *Nanoscale* **2014**, *6*, 2345.
[66] H. Lee, B. Seong, H. Moon, D. Byun, *RSC Adv.* **2015**, *5*, 28379.
[67] J. Lee, S. Kim, J. Lee, D. Yang, B. C. Park, S. Ryu, I. Park, *Nanoscale* **2014**, *6*, 11932.
[68] J. Lee, D. Yang, S. Kim, I. Park, *Solid-State Sensors, Actuators Microsystems (TRANSDUCERS & EUROSENSORS XXVII)*, IEEE, Picastaway, NJ, USA **2013**, 2624.
[69] M. Zheng, W. Li, M. Xu, N. Xu, P. Chen, M. Han, B. Xie, *Nanoscale* **2014**, *6*, 3930.
[70] D. Kang, P. V. Pikhitsa, Y. W. Choi, C. Lee, S. S. Shin, L. Piao, B. Park, K.-Y. Suh, T.-i. Kim, M. Choi, *Nature* **2014**, *516*, 222.
[71] C. Lee, L. Jug, E. Meng, *Appl. Phys. Lett.* **2013**, *102*, 183511.
[72] S. Luo, T. Liu, *Adv. Mater.* **2013**, *25*, 5650.
[73] S.-H. Hwang, H. W. Park, Y.-B. Park, M.-K. Um, J.-H. Byun, S. Kwon, *Composites Sci. Technol.* **2013**, *89*, 1.
[74] S. Gong, D. Lai, Y. Wang, L. W. Yap, K. J. Si, Q. Shi, N. N. Jason, T. Sridhar, H. Uddin, W. Cheng, *ACS Appl. Mater. Interfaces* **2015**, *7*, 19700.
[75] B.-U. Hwang, J.-H. Lee, T. Q. Trung, E. Roh, D.-I. Kim, S.-W. Kim, N.-E. Lee, *ACS Nano* **2015**, *9*, 8801.
[76] X. Li, R. Zhang, W. Yu, K. Wang, J. Wei, D. Wu, A. Cao, Z. Li, Y. Cheng, Q. Zheng, *Sci. Rep.* **2012**, *2*, 870.
[77] H. Deng, M. Ji, D. Yan, S. Fu, L. Duan, M. Zhang, Q. Fu, *J. Mater. Chem. A* **2014**, *2*, 10048.
[78] W. Obitayo, T. Liu, *Carbon* **2014**, *85*, 372.
[79] W. Hu, X. Niu, R. Zhao, Q. Pei, *Appl. Phys. Lett.* **2013**, *102*, 083303.
[80] H. Eom, J. Lee, A. Pichitpajongkit, M. Amjadi, J. H. Jeong, E. Lee, J. Y. Lee, I. Park, *Small* **2014**, *10*, 4171.
[81] L. Wang, Y. Li, *IEEE Trans. Instrum. Meas.* **2013**, *62*, 495.
[82] J. Zhao, C. He, R. Yang, Z. Shi, M. Cheng, W. Yang, G. Xie, D. Wang, D. Shi, G. Zhang, *Appl. Phys. Lett.* **2012**, *101*, 063112.
[83] F. Xu, Y. Zhu, *Adv. Mater.* **2012**, *24*, 5117.
[84] S. Yun, X. Niu, Z. Yu, W. Hu, P. Brochu, Q. Pei, *Adv. Mater.* **2012**, *24*, 1321.
[85] S. Park, M. Vosguerichian, Z. Bao, *Nanoscale* **2013**, *5*, 1727.
[86] D. J. Lipomi, M. Vosgueritchian, B. C. Tee, S. L. Hellstrom, J. A. Lee, C. H. Fox, Z. Bao, *Nat. Nanotechnol.* **2011**, *6*, 788.
[87] O. Kanoun, C. Müller, A. Benchirouf, A. Sanli, T. N. Dinh, A. Al-Hamry, L. Bu, C. Gerlach, A. Bouhamed, *Sensors* **2014**, *14*, 10042.
[88] B. Sun, Y.-Z. Long, Z.-J. Chen, S.-L. Liu, H.-D. Zhang, J.-C. Zhang, W.-P. Han, *J. Mater. Chem. C* **2014**, *2*, 1209.
[89] S. Yao, Y. Zhu, *Adv. Mater.* **2015**, *27*, 1480.
[90] Z. Jing, Z. Guang-Yu, S. Dong-Xia, *Chin. Phys. B* **2013**, *22*, 057701.
[91] A. A. Barlian, W.-T. Park, J. R. Mallon, A. J. Rastegar, B. L. Pruitt, *Proc. IEEE* **2009**, *97*, 513.
[92] J. Zhou, Y. Gu, P. Fei, W. Mai, Y. Gao, R. Yang, G. Bao, Z. L. Wang, *Nano Lett.* **2008**, *8*, 3035.
[93] J. Cao, Q. Wang, H. Dai, *Phys. Rev. Lett.* **2003**, *90*, 157601.
[94] R. He, P. Yang, *Nat. Nanotechnol.* **2006**, *1*, 42.
[95] C. Stampfer, A. Jungen, R. Linderman, D. Obergfell, S. Roth, C. Hierold, *Nano Lett.* **2006**, *6*, 1449.
[96] Y. Lee, S. Bae, H. Jang, S. Jang, S.-E. Zhu, S. H. Sim, Y. I. Song, B. H. Hong, J.-H. Ahn, *Nano Lett.* **2010**, *10*, 490.
[97] M. Hanay, S. Kelber, A. Naik, D. Chi, S. Hentz, E. Bullard, E. Colinet, L. Duraffourg, M. Roukes, *Nat. Nanotechnol.* **2012**, *7*, 602.
[98] J. Chaste, A. Eichler, J. Moser, G. Ceballos, R. Rurali, A. Bachtold, *Nat. Nanotechnol.* **2012**, *7*, 301.
[99] X.-W. Fu, Z.-M. Liao, J.-X. Zhou, Y.-B. Zhou, H.-C. Wu, R. Zhang, G. Jing, J. Xu, X. Wu, W. Guo, *Appl. Phys. Lett.* **2011**, *99*, 213107.
[100] A. Desai, M. Haque, *Thin-Walled Structures* **2005**, *43*, 1787.
[101] X. Li, H. Gao, C. J. Murphy, K. Caswell, *Nano Lett.* **2003**, *3*, 1495.
[102] K. Keshoju, L. Sun, *J. Appl. Phys.* **2009**, *105*, 023515.
[103] J. Park, Y. Lee, J. Hong, Y. Lee, M. Ha, Y. Jung, H. Lim, S. Y. Kim, H. Ko, *ACS Nano* **2014**, *8*, 12020.
[104] H. Tian, Y. Shu, Y.-L. Cui, W.-T. Mi, Y. Yang, D. Xie, T.-L. Ren, *Nanoscale* **2013**, *6*, 699.
[105] S. Gong, D. T. Lai, B. Su, K. J. Si, Z. Ma, L. W. Yap, P. Guo, W. Cheng, *Adv. Electron. Mater.* **2015**, *1*, 1400063.
[106] M. Li, H. Li, W. Zhong, Q. Zhao, D. Wang, *ACS Appl. Mater. Interfaces* **2014**, *6*, 1313.
[107] C. Li, E. T. Thostenson, T.-W. Chou, *Appl. Phys. Lett.* **2007**, *91*, 223114.
[108] B. De Vivo, P. Lamberti, G. Spinelli, V. Tucci, L. Vertuccio, V. Vittoria, *J. Appl. Phys.* **2014**, *116*, 054307.
[109] A. B. Oskouyi, U. Sundararaj, P. Mertiny, *Materials* **2014**, *7*, 2501.
[110] J. Hicks, A. Behnam, A. Ural, *Appl. Phys. Lett.* **2009**, *95*, 213103.
[111] J. Zhao, K. Dai, C. Liu, G. Zheng, B. Wang, C. Liu, J. Chen, C. Shen, *Composites Part A* **2013**, *48*, 129.
[112] S. Gong, Z. H. Zhu, *Polymer* **2014**, *55*, 4136.
[113] K. K. Kim, S. Hong, H. M. Cho, J. Lee, Y. D. Suh, J. Ham, S. H. Ko, *Nano Lett.* **2015**, *15*, 5240.
[114] A. Oliva-Avilés, F. Avilés, V. Sosa, *Carbon* **2011**, *49*, 2989.
[115] T. K. Kim, J. K. Kim, O. C. Jeong, *Microelectron. Eng.* **2011**, *88*, 1982.
[116] R. Zhang, H. Deng, R. Valenca, J. Jin, Q. Fu, E. Bilotti, T. Peijs, *Composites Sci. Technol.* **2013**, *74*, 1.
[117] R. Van Gastel, A. J. Martínez-Galera, J. Coraux, H. Hattab, D. Wall, F.-J. M. zu Heringdorf, M. Horn-von Hoegen, J. M. Gómez-Rodríguez, B. Poelsema, C. Busse, *New J. Phys.* **2009**, *11*, 113056.
[118] M. Zu, Q. Li, Y. Zhu, Y. Zhu, G. Wang, J.-H. Byun, T.-W. Chou, *Carbon* **2013**, *52*, 347.
[119] W. Bao, S. Meguid, Z. Zhu, G. Weng, *J. Appl. Phys.* **2012**, *111*, 093726.
[120] S. Xu, O. Rezvanian, M. Zikry, *J. Eng. Mater. Technol.* **2013**, *135*, 021014.
[121] S. Gong, Z. Zhu, E. Haddad, *J. Appl. Phys.* **2013**, *114*, 074303.
[122] W. Lu, T.-W. Chou, E. T. Thostenson, *Appl. Phys. Lett.* **2010**, *96*, 223106.
[123] I. Kang, M. J. Schulz, J. H. Kim, V. Shanov, D. Shi, *Smart Mater. Struct.* **2006**, *15*, 737.
[124] J. Zhang, J. Liu, R. Zhuang, E. Mäder, G. Heinrich, S. Gao, *Adv. Mater.* **2011**, *23*, 3392.
[125] D. Lee, H. P. Hong, M. J. Lee, C. W. Park, N. K. Min, *Sens. Actuators, A* **2012**, *180*, 120.
[126] X. Yang, Z. Zhou, F. Zheng, M. Zhang, J. Zhang, Y. Yao, *Solid-State Sensors, Actuators Microsystems Conf., 2009*, IEEE, Picastaway, NJ, USA **2009**, 1493.
[127] S. Patel, H. Park, P. Bonato, L. Chan, M. Rodgers, *J. Neuroeng. Rehabil.* **2012**, *9*, 21.
[128] M. M. Rodgers, V. M. Pai, R. S. Conroy, *IEEE Sens. J.* **2015**, *15*, 3119.
[129] R. Poppe, *Image Vision Comput.* **2010**, *28*, 976.
[130] S. S. Rautaray, A. Agrawal, *Artificial Intelligence Review* **2012**, *43*, 1.
[131] E. Roh, B.-U. Hwang, D. Kim, B.-Y. Kim, N.-E. Lee, *ACS Nano* **2015**, *9*, 6252.
[132] A. P. Gerratt, H. O. Michaud, S. P. Lacour, *Adv. Funct. Mater.* **2015**, *25*, 2287.
[133] Z. Liu, S. Fang, F. Moura, J. Ding, N. Jiang, J. Di, M. Zhang, X. Lepró, D. Galvão, C. Haines, *Science* **2015**, *349*, 400.
[134] F. Xu, X. Wang, Y. Zhu, Y. Zhu, *Adv. Funct. Mater.* **2012**, *22*, 1279.
[135] P. Mostafalu, W. Lenk, M. Dokmeci, B. Ziaie, A. Khademhosseini, S. Sonkusale, *Biomed. Circuits Systems Conf. (BioCAS)*, IEEE, Picastaway, NJ, USA **2014**, pp 456.
[136] S. Xu, Y. Zhang, L. Jia, K. E. Mathewson, K.-I. Jang, J. Kim, H. Fu, X. Huang, P. Chava, R. Wang, *Science* **2014**, *344*, 70.

[137] C. Meng, C. Liu, L. Chen, C. Hu, S. Fan, *Nano Lett.* **2010**, *10*, 4025.
[138] J. Kim, A. Banks, H. Cheng, Z. Xie, S. Xu, K. I. Jang, J. W. Lee, Z. Liu, P. Gutruf, X. Huang, *Small* **2015**, *11*, 906.
[139] S. Xu, Y. Zhang, J. Cho, J. Lee, X. Huang, L. Jia, J. A. Fan, Y. Su, J. Su, H. Zhang, *Nat. Commun.* **2013**, *4*, Article number: 1543.
[140] M. F. El-Kady, V. Strong, S. Dubin, R. B. Kaner, *Science* **2012**, *335*, 1326.
[141] L. Y. Chen, B. C.-K. Tee, A. L. Chortos, G. Schwartz, V. Tse, D. J. Lipomi, H.-S. P. Wong, M. V. McConnell, Z. Bao, *Nat. Commun.* **2014**, *5*, Article number: 5028.
[142] M. Sitti, R. S. Fearing, *J. Adhes. Sci. Technol.* **2003**, *17*, 1055.
[143] S. Kim, M. Sitti, *Appl. Phys. Lett.* **2006**, *89*, 261911.
[144] M. P. Murphy, B. Aksak, M. Sitti, *Small* **2009**, *5*, 170.
[145] P. Glass, H. Chung, N. R. Washburn, M. Sitti, *Langmuir* **2009**, *25*, 6607.
[146] Y.-L. Park, C. Majidi, R. Kramer, P. Bérard, R. J. Wood, *J. Micromech. Microeng.* **2010**, *20*, 125029.
[147] X. Liang, S. A. Boppart, *IEEE Trans. Biomed. Eng.* **2010**, *57*, 953.
[148] C. Pailler-Mattei, S. Bec, H. Zahouani, *Med. Eng. Phys.* **2008**, *30*, 599.